Biophysical Journal
Article

Biophysical Society

Two Pools of Vesicles Associated with Synaptic Ribbons Are Molecularly Prepared for Release

Proleta Datta,[1,2] Jared Gilliam,[1] Wallace B. Thoreson,[3,4] Roger Janz,[1,2] and Ruth Heidelberger[1,2,*]
[1]Department of Neurobiology and Anatomy, McGovern Medical School, University of Texas Health Science Center at Houston (UTHealth), Houston, Texas; [2]The University of Texas MD Anderson Cancer Center, UTHealth Graduate School of Biomedical Sciences, Houston, Texas; [3]Truhlsen Eye Institute, Department of Ophthalmology and Visual Sciences and [4]Department of Pharmacology and Experimental Neuroscience, University of Nebraska Medical Center, Omaha, Nebraska

ABSTRACT Neurons that form ribbon-style synapses are specialized for continuous exocytosis. To this end, their synaptic terminals contain numerous synaptic vesicles, some of which are ribbon associated, that have difference susceptibilities for undergoing Ca^{2+}-dependent exocytosis. In this study, we probed the relationship between previously defined vesicle populations and determined their fusion competency with respect to SNARE complex formation. We found that both the rapidly releasing vesicle pool and the releasable vesicle pool of the retinal bipolar cell are situated at the ribbon-style active zones, where they functionally interact. A peptide inhibitor of SNARE complex formation failed to block exocytosis from either pool, suggesting that these two vesicle pools have formed the SNARE complexes necessary for fusion. By contrast, a third, slower component of exocytosis was blocked by the peptide, as was the functional replenishment of vesicle pools, indicating that few vesicles outside of the ribbon-style active zones were initially fusion competent. In cone photoreceptors, similar to bipolar cells, fusion of the initial ribbon-associated synaptic vesicle cohort was not blocked by the SNARE complex-inhibiting peptide, whereas a later phase of exocytosis, attributable to the recruitment and subsequent fusion of vesicles newly arrived at the synaptic ribbons, was blocked. Together, our results support a model in which stimulus-evoked exocytosis in retinal ribbon synapses is SNARE-dependent; where vesicles higher up on the synaptic ribbon replenish the rapidly releasing vesicle pool; and at any given time, there are sufficient SNARE complexes to support the fusion of the entire ribbon-associated cohort of vesicles. An important implication of these results is that ribbon-associated vesicles can form intervesicular SNARE complexes, providing mechanistic insight into compound fusion at ribbon-style synapses.

INTRODUCTION

Ribbon-style active zones are specialized synapses that are found in neurons that relay sensory information in a continuous or analog manner. These active zones are marked by the presence of electron dense structures, the synaptic ribbons, to which a number of synaptic vesicles are tethered (1,2). Typically, only a fraction of the ribbon-tethered vesicles is located near the plasma membrane, whereas the majority face into the cytosol. In addition to a ribbon-tethered pool, there is usually a large number of cytoplasmic vesicles in the synaptic endings, some of which can appose the plasma membrane, where they may undergo fusion at nonribbon sites (3–7). Although the synaptic ribbons have been suggested to be a site at which vesicles become prepared for rapid, Ca^{2+}-dependent exocytosis (5,8,9), little is known about how ribbon-tethered vesicles located on upper rows of the ribbons and distant from the plasma membrane might become molecularly prepared for release, as this type of priming is typically understood to involve the formation of SNARE complexes between synaptic vesicles and the presynaptic plasma membrane.

Exocytosis at ribbon-style synapses occurs with several phases that can be distinguished on the basis of well-defined physiological characteristics (10–12). The fastest component of exocytosis is comprised of a relatively small number of vesicles that are released with minimal delay upon activation of voltage-gated Ca^{2+} channels (13–15). The fusion of vesicles in this rapidly releasing vesicle pool (RRP) gives rise to the fast transient component of the excitatory postsynaptic potential in downstream neurons. Multiple lines of evidence indicate that RRP vesicles are located on the lower rows of the synaptic ribbons, in close proximity to

Submitted May 2, 2017, and accepted for publication August 7, 2017.

*Correspondence: ruth.heidelberger@uth.tmc.edu

Proleta Datta's present address is University of California San Francisco, San Francisco, California.

Jared Gilliam's present address is University of Texas MD Anderson Cancer Center, Houston, Texas.

Editor: Edward Stuenkel.

http://dx.doi.org/10.1016/j.bpj.2017.08.012

the presynaptic membrane and voltage-gated Ca^{2+} channels (1,14,16,17). A secondary population of vesicles, termed the "releasable pool" (RP), contributes to a slower, more sustained component of stimulus-evoked release (1,15,18–21). Although its location has been debated, like the RRP, the RP requires the presence of functional synaptic ribbons (5,22) and in the retina, its magnitude generally agrees with the number of ribbon-tethered vesicles (2,16,23,24). There are also later components of release that may contain contributions from the fusion of vesicles at ectopic, non-ribbon sites or even involve a different Ca^{2+} sensor (3,4,6,7,25–27). Although RRP vesicles are prepared for the rapid, Ca^{2+}-dependent fusion at retinal ribbon-style synapses, the molecular readiness of other components of release to participate in stimulus-evoked exocytosis is unknown.

We examined Ca^{2+}-dependent, stimulus-evoked exocytosis from retinal bipolar cells and photoreceptors, two classes of neuron that form ribbon-style synapses. Under conditions previously demonstrated to block functional vesicle pool replenishment, we first demonstrated that the RRP and the RP in bipolar cells functionally interact in a manner that is consistent with a major role for RP vesicles in the replenishment of the RRP vesicle pool. We then showed that the fusion of vesicles in either vesicle pool was not inhibited by addition of a SNARE complex-inhibiting peptide, whereas a later component of release, presumed to arise from the recruitment of new vesicles to the fusion-competent state, was. That vesicles in the initial RP were not inhibited by the peptide was a puzzling finding given their proposed location on the synaptic ribbons, which places them at a distance of one or more vesicle diameters ($\geq$30 nm) from the plasma membrane. Similar results were observed in cone photoreceptors, where the SNARE complex-inhibiting peptide did not affect exocytosis of vesicles initially associated with the synaptic ribbons, but it did inhibit the fusion of new recruits to the synaptic ribbons. We propose a model of retinal ribbon synapse function in which stimulus-evoked exocytosis in retinal ribbon synapses is SNARE-dependent, continuous release is supported by the sequential recruitment of vesicles, and the synaptic ribbon serves as a nidus for SNARE-dependent vesicle priming.

METHODS

Animal care

Goldfish, 4–5″ in length, were obtained from an approved supplier (Ozark Fisheries, Martinsville, IN). All goldfish procedures conformed to the National Institute of Health guidelines and were approved by the Animal Welfare Committee of the University of Texas Medical School at Houston. Goldfish were maintained on a 12-h light/dark cycle and sacrificed after $\geq$1 h of dark adaptation. Euthanization was by decapitation followed by pithing.

Aquatic tiger salamanders (*Ambystoma tigrinum*, 18–25 cm; Sullivan Company, Nashville, TN) were maintained on a 12-h light/dark cycle and sacrificed after $\geq$1 h of dark adaptation. Salamanders were anesthetized by immersion in 0.25 g/L tricaine methanesulfonate (Tricaine-S; Western Chemical, Ferndale, WA) for >15 min, decapitated with heavy shears, and then pithed. Salamander procedures were approved by the University of Nebraska Medical Center Institutional Animal Care and Use Committee.

Preparation of isolated retinal bipolar cell synaptic terminals

Acutely isolated synaptic terminals from goldfish Mb1 bipolar cells were prepared as described previously (28). In brief, dark-adapted goldfish, 4–5″ in length, were euthanized, and eyes were opened in chilled, oxygenated, low-calcium external solution containing 120 mM NaCl, 2.6 mM KCl, 1.0 mM $MgCl_2$, 0.5 mM $CaCl_2$, 10 mM HEPES, 10 mM Glucose, pH 7.3, 260 mOsm. The retinas were dissected free and cut into 8–10 pieces and incubated for 30 min at 20°C in a digestion solution containing 115 mM NaCl, 2.5 mM KCl, 1.0 Mm $MgCl_2$, 0.5 mM $CaCl_2$, 10 mM PIPES, 10 mM Glucose, 2.7 mM Cysteine, to which Papain was added at 30 U/mL (Fluka, Steinheim, Germany or Sigma-Aldrich, St. Louis, MO) or 150,000 USP U/mL (Calbiochem, Billerica, MA). The final pH was 7.25–7.30, and the final osmolarity was 260–265 mOsm. After digestion, pieces were rinsed and stored for up to 8 h in oxygenated, low-calcium external solution at 10°C. Bipolar cell terminals were isolated from pieces as needed by mechanical trituration with a fire-polished Pasteur pipette and plated onto clean glass coverslips. They were allowed to settle for 15–30 min before use.

Preparation of salamander retinal slices

A detailed description of retinal slice preparation and whole cell recording techniques has been published elsewhere (29). Briefly, after enucleation, the front of the eye was removed and the resulting eyecup was cut into 2–4 pieces. A piece of retina was placed vitreal side down on a piece of nitrocellulose membrane (5 × 10 mm; type AAWP, 0.8 μm pores; EMD Millipore, Billerica, MA). The filter paper was submerged in cold amphibian saline and the sclera was peeled away, leaving the retina adhering to the membrane. The retina was cut into 125-μm slices using a razor blade tissue slicer (Stoelting, Wood Dale, IL). Slices were rotated 90° to view retinal layers and anchored in the recording chamber by embedding the ends of the nitrocellulose membrane in vacuum grease. The recording chamber was mounted on an upright fixed-stage microscope (Olympus BH2-WI; Tokyo, Japan). Slices were superfused at ~1 mL min^{-1} with oxygenated normal amphibian saline solution containing 116 mM NaCl, 2.5 mM KCl, 1.8 mM $CaCl_2$, 0.5 mM $MgCl_2$, 5 mM glucose, and 10 mM HEPES (pH 7.8).

Electrophysiological recordings in bipolar cell synaptic terminals

The external solution contained 120 mM NaCl, 2.6 mM KCl, 1.0 mM $MgCl_2$, 2.5 mM $CaCl_2$, 10 mM HEPES, 10 mM Glucose, pH 7.3, 260 mOsm. Whole-terminal recordings were made using Sylgard-coated (Dow Corning, Corning, NY) pipettes, 5–7 MΩ, pulled from unfilamented borosilicate glass. To minimize potential differences in intraterminal Ca^{2+} concentration that could influence vesicle recruitment and functional pool refilling, the free Ca^{2+} concentration in the base internal solution was defined by use of a Ca^{2+}-EGTA buffered internal solution (9,30). This defined the intracellular Ca^{2+} concentration at ~150 nM, as calculated by Maxchelator (http://maxchelator.stanford.edu) and experimentally confirmed with quantitative measurement of bis-fura2 fluorescence. Free EGTA was calculated to be ~2.4 mM, approximating the endogenous buffering capacity of these neurons (31,32).

The base internal solution for the ATP/ATP-γS comparison experiments contained 100 mM CsGluconate, 10 mM TEA, 3.0 mM $MgCl_2$, 5 mM

EGTA, 2.5 mM $CaCl_2$, 35 mM HEPES, 2mM Na_2ATP, 0.5 mM GTP 0.5, and 0.1 mM bis-fura-2, pH 7.25–7.3, 265–275 mOsm. The base internal recording solution for the peptide- and peptide-free experiments was identical except that: 1) the concentration of $MgCl_2$ was increased to 6 mM, 2) the concentration of Na_2ATP was increased to 5 mM, and 3) bis-fura-2 was omitted. To block functional pool refilling, ATP-γS replaced ATP in the control pipette solution (8,9,33). To isolate the rapidly releasing vesicle pool (14,17,34), the total EGTA concentration was increased by 5 mM, yielding a calculated free EGTA concentration of ~4.7 mM (Maxchelator).

Capacitance measurements were performed using a computer-controlled EPC-9 patch-clamp amplifier running Pulse software (HEKA Electronik, Lambrecht, Germany). A sine-wave voltage command (805 Hz, 30 mV peak–to-peak) was applied about a holding potential of −60 mV (8,9,35) and the resultant signal processed using the Lindau-Neher technique (36,37) to give estimates of the membrane capacitance (C_m), series conductance (G_s), and membrane conductance (G_m). High-resolution measurements were performed at 805 Hz for 100 ms immediately before each stimulus train and for 50 ms after each voltage step in the train. In addition, C_m, G_s, and G_m were monitored at 10 Hz before and between stimulus trains and before and after isolated membrane depolarizations. Recordings from terminals with $G_s < 50$ nS, current at holding potential >-40 pA, or ΔC_m changes <1 SD above baseline were excluded from the final data set. ΔC_{m1} was defined as the magnitude of the capacitance change evoked by the first pulse in the train and $\Delta C_{m\text{total}}$ was defined as the total cumulative capacitance increase at the end of the pulse train averaged over the last five stimuli in the train. The amplitude of the presynaptic calcium current, I_{Ca}, was determined from measurement of the last 5 ms of each 20-ms depolarization. I_{Ca1} was defined as the magnitude of I_{Ca} elicited by the first depolarizing voltage step in the stimulus train. I_{Ca136} was defined as the average I_{Ca} evoked by the last five voltage steps in the stimulus train.

Electrophysiological recordings in salamander retinal slices

Patch pipettes were fabricated with borosilicate glass (1.2 mm OD, 0.9 mm ID, with an internal filament; World Precision Instruments, Sarasota, FL) using a PC-10 or PP-830 vertical puller (Narishige, East Meadow, NY). Patch pipettes had tip diameters of ~1 μm and resistances of 15–20 MΩ. The pipette solution for cones contained 50 mM Cs-gluconate, 40 mM Cs-glutamate, 10 mM TEA-Cl, 3.5 mM NaCl, 1 mM $CaCl_2$, 1 mM $MgCl_2$, 10 mM ATP-Mg, 0.5 mM GTP-Na, 10 mM HEPES, and 5 mM EGTA. The addition of glutamate to the presynaptic pipette solution enhances synaptic currents and slows rundown in whole-cell recordings (38). The pipette solution for horizontal cell pipettes was identical except that the 40 mM Cs-glutamate was replaced with an additional 40 mM Cs-gluconate. Reported voltage values were not corrected for a measured liquid junction potential of 9 mV.

Synaptic transmission was monitored using paired whole-cell recordings from cones and horizontal cells. Cones were identified by their characteristic morphology. Horizontal cells were identified by their morphology, position in the slice, and electrophysiological characteristics (29). Horizontal cells were voltage-clamped at −60 mV and cones at −70 mV with a Multiclamp 700A amplifier (Molecular Devices, Sunnyvale, CA). We targeted cones and horizontal cells positioned adjacent to one another in the slice. Signals were digitized at 10 kHz with a Digidata 1322A A:D/D:A interface (Molecular Devices) and low-pass filtered with a cutoff of 2 kHz. Recordings were excluded if the cone access resistance exceeded 60 MΩ or changed dramatically over the course of the recording or if the cone holding current at −70 mV exceeded 300 pA. Properties of release from cones were evaluated using pulse trains as described in the results. The increase in charge transfer Q_{PSC} caused by spontaneous release, largely due to spontaneous release from neighboring photoreceptors that were not voltage-clamped, was assessed during a 2-s baseline period before the onset of the train and subtracted out.

Peptides and peptide handling

The syntaxin3B peptide (NH2-RHKDIMRLESSIKELHDMFVDVA-OH), stx3pep, was derived from the N-terminal half of the SNARE domain of goldfish syntaxin3B and contained two conserved changes (39). The control peptide (NH2- RIALKDDVIHMRESVDHKSFMEL-OH), stx3con, contained the same amino acids as stx3pep, but they were arranged in a different order (39). To allow visualization of peptide diffusion from the peptide solution into a synaptic terminal, the peptides were labeled with fluorescein isothiocyanate (FITC) at their N termini using an AHX linker. Peptides were synthesized by Biosynthesis (Lewisville, TX) at >95% purity. Entry of FITC tagged-peptides into the bipolar cell synaptic terminal was monitored using a computer-controlled, monochromator-based photometry system (39–41). The time constant (τ) of loading in bipolar cell terminals was similar for both peptides (stx3pep: $\tau = 89 \pm 11$ s ($n = 6$); stx3con $\tau = 87 \pm 14$ s ($n = 4$); $p > 0.9$) and indicated that after achieving the whole-terminal recording configuration, equilibrium between the pipette and terminal took several minutes to attain for both peptides. For cone photoreceptors, 7 min were allowed after achieving the whole-cell recording configuration for the peptides to reach equilibrium (42) before presenting the first stimulus.

For bipolar cell experiments, a 500 μM stock peptide solution by weight was made using the base internal recording solution for peptide experiments described in a preceding section. The solution was then filtered through a 0.2 μm PES filter (Nalgene; Nalge Nunc, Thermo Fisher Scientific, Waltham, MA) to remove any undissolved solutes. On the day of an experiment, the resultant stock solution was diluted with an equal volume of peptide-free internal solution to yield a final nominal peptide concentration of 250 μM. The final osmolarity was adjusted to 270–274 mOsm with MQ water, as needed. The peptide-containing solutions for use in cone photoreceptors were prepared in a similar fashion using a photoreceptor-appropriate base internal solution with a final nominal concentration of 250 μM. The concentration of the FITC-labeled peptide in the final bipolar cell internal solutions was calculated from the optical density measured at 494 nm and using the extinction coefficient for FITC. The calculations suggested that final concentrations were actually closer to ~130 μM for the control peptide, stx3con, and ~165 μM for the syntaxin3B SNARE-binding domain peptide, stx3pep. The decrement in concentration from that predicted is likely due to retention of peptide in the filter, in addition to contributions of nonlabeled peptide and peptide fragments.

In vitro protein assay

Goldfish retina was homogenized in a buffer containing 1% Triton-X-100 and centrifuged. The supernatant was mixed with the peptide derived from syntaxin3B, stx3pep, or the scrambled control peptide, stx3con, at a final peptide concentration 0.5 μM and incubated for 2 h at room temperature. The samples were then mixed with SDS-sample buffer, separated by SDS-PAGE without boiling of the samples, and analyzed by Western blot with a syntaxin3 antibody (39).

Analysis

Analysis of capacitance, conductance, and calcium concentration was performed in the software Igor Pro (WaveMetrics, Portland, OR). Statistical analysis of bipolar cell data was performed using Student's unpaired *t*-test in the software Excel (Microsoft, Mountain View, CA) or via ANOVA using StatPlus:Mac LE, Version 2009 (AnalystSoft, http://www.analystsoft.com). The normalized capacitance response as a function of train number (Figs. 6 *B* and 7 *B*) was analyzed using a mixed effect model in SAS for Windows (v9.4; SAS Software, Cary, NC). Analysis of data obtained from paired recordings in retinal slices was performed using GraphPad Prism 4 (GraphPad, La Jolla, CA). For physiological experiments, *n* equals the number of synaptic terminals or cone photoreceptors examined.

Data were analyzed without regard to experimental condition. Data are expressed as mean ± SE, except where noted. The recordings within a cohort always contained data from multiple animals. Control data were obtained from contemporaneous experiments interleaved with test experiments. For all figures, a p-value < 0.05 was considered significant and denoted by *. A p-value < 0.005 was indicated by **.

RESULTS

A stimulus train captures the fusion of vesicles originating from different pools

Using the synaptic terminal of the goldfish bipolar cell as a model preparation, we designed a stimulus train that allowed us to examine exocytosis over a ~10-s time window and visualize the contributions made by the previously defined RRP and the RP to the secretory response. In addition, the train was designed to capture the contributions of other vesicles, such as those that might fuse at distant, non-ribbon sites and new recruits that replenish ribbon-associated vesicle pools. Exocytosis was measured using a combination of time-resolved and high-resolution membrane capacitance measurements (43). Fig. 1 *A* shows a representative high-resolution capacitance response of an isolated synaptic terminal to the stimulus train. In this example, there was an initial jump in membrane capacitance of ~30 fF in response to the first 20-ms voltage step (−60 to 0 mV) in the train, consistent with the fusion of vesicles in the RRP (14). This was followed by steady rise in membrane capacitance in response to each stimulus of the train, yielding a total increase in C_m of ~200 fF. Fig. 1 *B* shows the presynaptic Ca^{2+} current (I_{Ca}) and high-resolution records for membrane capacitance (C_m) and conductance (G_s and G_m) evoked by the first depolarizing voltage step of the train on an expanded timescale. The capacitance record reveals a sustained, stimulus-evoked jump in C_m that was not correlated with changes in the conductance traces G_s and G_m. To avoid potential effects of a stimulus-evoked transient change in G_s and G_m on the calculation of C_m, the first 20 ms of the capacitance record after each depolarization were excluded from analysis (37,43–45). Endocytosis was not observed in the 50-ms interval between depolarizing voltage steps (e.g., Fig. 1 *B*) and during the pulse train, the spatially averaged intraterminal calcium exceeded 500 nM (data not shown), a concentration at which endocytosis is inhibited in goldfish retinal bipolar cells (30,46,47). Thus, we interpret net changes in membrane capacitance measured during the stimulus train to primarily reflect exocytosis.

We next determined the identity of the vesicle populations that contributed to the train-evoked capacitance increase. To reveal the RRP, we prevented the fusion of vesicles outside of the RRP by elevating the free concentration of the slow Ca^{2+}-buffer EGTA in the internal recording solution to ~5 mM (14,17,34). Fig. 2 compares the mean cumulative capacitance response, $\Delta C_{m\text{total}}$, evoked by the stimulus train under control conditions (*open circles*) and in the presence of ~5 mM free EGTA (*solid circles*). With ~5 mM free EGTA in the internal recording solution, $\Delta C_{m\text{total}}$ decreased from a mean value of 233 ± 48 fF ($n = 6$) to a mere 53 ± 20 fF ($n = 4$) ($p << 0.001$). This reduction in total exocytosis was not attributable to a reduction in Ca^{2+} current amplitude, I_{Ca}, as there was no difference in I_{Ca} evoked by the first depolarization in the train, I_{Ca1}, nor in the mean amplitude of I_{Ca} measured at the end of the stimulus train, I_{Ca136}, between control and high EGTA terminals (Control: $I_{Ca1} = -172 \pm 32$ pA ($n = 6$); ~5 mM EGTA: $I_{Ca1} = -167 \pm 34$ pA, ($n = 5$), $p > 0.9$; Control: $I_{Ca136} = -108 \pm 6$ pA ($n = 6$); ~5 mM EGTA: $I_{Ca136} = -113 \pm 18$ pA, ($n = 4$), $p > 0.8$; data not shown). Importantly, ~5 mM free EGTA revealed a plateau early in the cumulative capacitance response that lasted for several seconds (Fig. 2, *solid circles*). The magnitude of this plateau, indicative of the RRP, was ~24 fF and similar

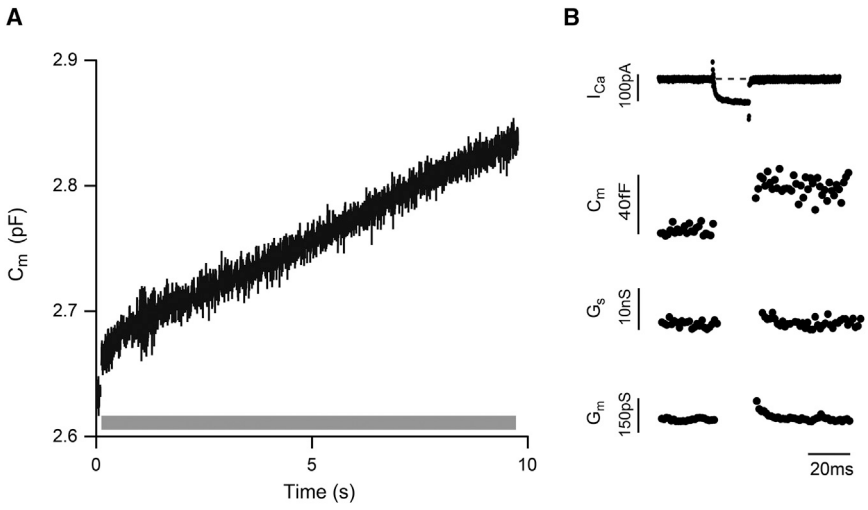

FIGURE 1 A stimulus train applied to a single synaptic terminal demonstrates that stimulus-evoked exocytosis can continue for seconds. (*A*) A high-resolution capacitance recording from an isolated bipolar cell synaptic terminal demonstrates that exocytosis is evoked throughout an ~10 s stimulus train. The stimulus train was comprised of 136 and 20-ms depolarizing voltage steps (−60 to 0 mV) with an interpulse interval of 50 ms. The shaded bar indicates the timing of the stimulus train. (*B*) A representative family of Ca^{2+} current (I_{Ca}), capacitance (C_m), series conductance (G_s) and membrane conductance (G_m) traces evoked by the first voltage step in the stimulus train is shown on an expanded timescale. Same terminal as in (*A*). Gaps in the C_m, G_s, and G_m traces correspond to the 20-ms period when Ca^{2+} channels were conducting, and thus, measurement of these parameters is unreliable (37,44). There were no correlated changes C_m, G_s, and G_m.

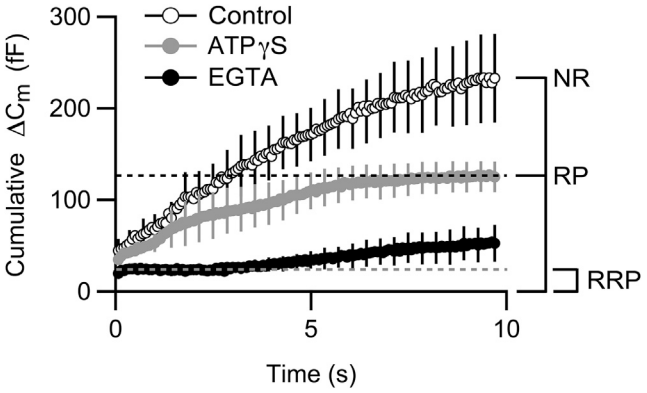

FIGURE 2 The capacitance response evoked by the stimulus train contains contributions from different vesicle pools. Control terminals, dialyzed with standard internal solution underwent stimulus-evoked exocytosis throughout the stimulus train (*open circles*, $n = 6$). The RRP was defined by dialyzing terminals with internal solution containing ~5 mM free EGTA (*solid circles*, $n = 4$). In the presence of ~5 mM EGTA, there was an initial secretory plateau that lasted ~2.5 s and had an amplitude of ~24 fF, indicative of the RRP. The RP was isolated by replacing ATP in the internal recording solution with ATPγS (*shaded circles*, $n = 7$) to prevent the functional refilling of the RP (8,9). In the presence of ATP-γS, $\Delta C_{m\text{total}}$ decreased from a control value of 233 ± 48 fF ($n = 6$) to 125 ± 17 fF ($n = 7$; $p < 0.05$). For ease of viewing, error bars are shown every fifth data point. NR refers to those vesicles that contributed to exocytosis that resided in neither the initial RRP nor RP.

to the 22 ± 3 fF ($n = 5$) capacitance increase evoked by the first stimulus in the train (Fig. 2). This correspondence suggests that the mean secretory response evoked by the first pulse in the train, ΔC_{m1}, provides a reasonable approximation of the RRP in these experiments. The slow rise in capacitance that followed the plateau most likely reflects additional exocytosis that occurred as the Ca^{2+} buffering capacity of EGTA was exceeded by the train-driven Ca^{2+} entry.

To isolate the RP and reveal the contributions to the exocytotic response from vesicles that initially resided outside of a fusion-competent vesicle pool, we replaced ATP in the internal recording solution with ATP-γS, a nonhydrolyzable ATP analog that inhibits a biochemical step necessary for the preparation of synaptic vesicles and/or release sites for Ca^{2+}-evoked fusion without affecting vesicle attachment to the synaptic ribbons or the final fusion step (8,9,33,48). To control for potential differences in basal Ca^{2+} secondary to reduced ATP levels that might affect the rates of pool replenishment (18,34,49), free Ca^{2+} was defined in control and ATP-γS internal solutions with the use of a Ca^{2+}-buffered internal recording solution (9,30). Fig. 2 shows that when ATP was replaced with ATPγS, the total extent of train-driven exocytosis decreased by nearly one-half relative to control, indicating an RP of ~125 fF (Control: $\Delta C_{m\text{total}} = 233 \pm 48$ fF ($n = 6$); ATP-γS: $\Delta C_{m\text{total}} = 125 \pm 16$ fF ($n = 7$); $p < 0.05$). The reduction in the total, train-evoked capacitance response was not readily attributable to a difference in I_{Ca} between the conditions. The amplitudes of the initial mean depolarization-evoked I_{Ca} were similar as were the amplitudes of the mean I_{Ca} measured at the end of the stimulus train (Control: $I_{Ca1} = -172 \pm 32$ pA ($n = 6$); ATP-γS: $I_{Ca1} = -139 \pm 16$ pA ($n = 7$); $p > 0.3$; Control: $I_{Ca136} = -108 \pm 6$ pA ($n = 6$); ATP-γS: $I_{Ca136} = -83 \pm 3$pA ($n = 7$) $p > 0.1$; data not shown). The lack of effect of ATP-γS on I_{Ca} is consistent with previous findings demonstrating that ATP-γS inhibits functional refilling of the RP by acting at a locus other than presynaptic Ca^{2+} signaling (8,9).

Together, the data suggest that in this cohort of cells, the RRP has an average amplitude of 25 fF and the RP has an average amplitude of 125 fF. These values are in good agreement to literature values for these pools and the 5:1 relationship noted between the RP and RRP in bipolar cells (2). In addition, the stimulus train evoked the fusion of ~100 fF worth of vesicles or fusion sites that were not initially in either pool. We refer to these vesicles as "new recruits" (NR) without speculating on their location of origin (e.g., new recruits to the synaptic ribbons versus nonribbon, ectopic fusion sites).

Demonstration of a functional relationship between the RRP and the RP

Although there is good evidence indicating that the RRP is located at the base of the synaptic ribbons nearest the clusters of presynaptic Ca^{2+} channels (1,50,51), the location of the RP is less clear. Some studies of ribbon-style synapses have suggested that the RP corresponds to the ribbon-tethered releasable pool (16,23,24,52), and have suggested that vesicles located higher up on the synaptic ribbon replace lower-row vesicles that were lost to fusion (1,34,53). However, exocytosis at nonribbon sites has also been reported at retinal ribbon-style synapses (3,4,6,51) that could potentially contribute to secondary components of release. The first scenario implies that the RP can be called upon to replenish the RRP, whereas in the second scenario, there would be little to no functional interaction between the two pools. To test for a functional relationship between the RRP and the RP, we asked whether depletion of the RRP could cross-deplete the RP.

The ability of the RRP to cross-deplete the RP was compared under control conditions and under conditions in which the functional replenishment of the RP was inhibited by ATP-γS. As above, the resting intraterminal Ca^{2+} concentration was defined with the use of a Ca^{2+}-buffered internal recording solution and did not significantly differ between control and ATP-γS terminals (Fig. 3 *A*). Depletion of the RRP was triggered by a brief, depolarizing voltage step (20 ms, −60 to 0 mV (14)). After a 30-s delay, a second, identical voltage step was given to probe the state of refilling. The delay was more than sufficient for the collapse of Ca^{2+} microdomains (54) and RRP replenishment under standard conditions (14). Additional depolarizing voltage steps were given, each separated by 30 s, until the stimulus

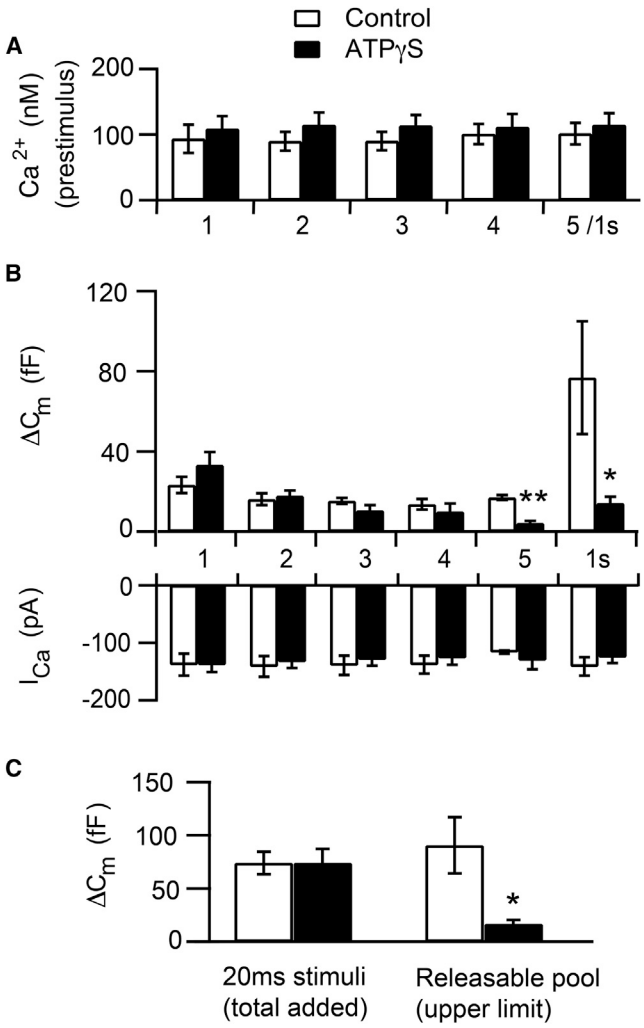

FIGURE 3 The RRP functionally interacts with the RP. (*A*). The resting intraterminal Ca^{2+} concentration was similar between control terminals (*open bars*) and ATP-γS terminals (*solid bars*). Data depicted are the mean, spatially averaged intraterminal Ca^{2+} values averaged over the 5-s period immediately before each 20-ms depolarization. Numbers below the *x* axis indicate the number of the 20-ms depolarization in the pulse sequence. The last value, 5/1 s, indicates the period immediately before the last 20-ms depolarization/1-s depolarization combination. (*B*) The upper panel shows the average capacitance response to each of the five 20-ms depolarizing voltage steps (−60 to 0 mV) in the sequence and the 1-s depolarization (−60 to 0 mV) used to probe the magnitude of the remaining RP. Lower panel shows the average magnitude of the corresponding Ca^{2+} currents. (*C*) (*Left*) The total membrane added by the series of 20-ms depolarizations was similar between control and ATP-γS terminals. (*Right*) The releasable pool remaining after four 20-ms pulses, given by the combined magnitude of the response to last 20-ms depolarization and the 1-s depolarization, was significantly smaller in terminals dialyzed with ATP-γS ($p < 0.008$). For (*A–C*), control terminals: $n = 6$. For ATP-γS terminals: For 1-s depolarizations, $n = 8$. For 20-ms depolarizations 1–3, $n = 8$; 20-ms depolarization 4, $n = 7$; and 20-ms depolarization 5, $n = 5$.

failed to evoke a response or five stimuli were given, whichever came first. Immediately after the final 20-ms depolarization, the RP was probed using a standard stimulus to tap the RP, a 1-s depolarization from −60 to 0 mV (8,9,19,52).

In control terminals, the RRP could be depleted and refilled multiple times (Fig. 3 *B*, *upper panel*, *open bars*). After five 20-ms pulses, the subsequent 1-s depolarization evoked an increase in membrane capacitance of 77 ± 28 fF ($n = 6$). By contrast, in ATP-γS terminals, despite comparable and adequate I_{Ca} (Fig. 3 *B*, *lower panel*), the ability to functionally refill the RRP diminished with successive stimulation (Fig. 3 *B*, *upper panel*, *black bars*). By a fifth 20-ms depolarization, the mean amplitude of the capacitance jump in ATP-γS terminals was <5 fF, indicating a near total cessation of functional refilling of the RRP. This result provides a sharp contrast to the ∼17 fF response observed in control terminals (Fig. 3 *B*; $p < 0.005$). Furthermore, the subsequent response to the 1-s depolarization was 14 ± 3 fF ($n = 8$), a value significantly smaller than the ∼77 fF response observed in control terminals ($p < 0.03$). The upper limit of the RP after four rounds of release, calculated from the combined magnitude of the final 20-ms depolarization and the 1-s depolarization, was reduced to ∼19% of its control value when refilling of the RP was inhibited (Fig. 3 *C*; Control: 91 ± 27 fF, $n = 6$; ATP-γS: 17 ± 4fF, $n = 8$; $p < 0.008$).

This strong cross-depletion of the RP by depletion of the RRP could not be attributed to a difference in the total amount of membrane added by the preceding 20-ms pulses, as this was virtually identical between control and ATP-γS terminals (Fig. 3 *C*). The apparent decrease in RP was also not attributable to smaller stimulus-evoked I_{Ca}, as these were similar between control and ATP-γS terminals (Fig. 3 *B*, *lower panel*), consistent with a lack of inhibition of I_{Ca} by ATP-γS (9). Finally, we note that the stimulus-evoked rise in the spatially averaged intraterminal Ca^{2+} evoked by the 1-s depolarization also did not differ significantly between control and test terminals (Control: ΔCa^{2+} = 539 ± 117 nM, $n = 5$; ATP-γS: ΔCa^{2+} = 466 ± 109 nM, $n = 8$, $p > 0.67$; data not shown). Taken together, the data demonstrate a functional interaction between the RRP and the RP. This interaction is consistent with a role for RP vesicles in replenishing the RRP, although other interpretations are possible (see Discussion).

A SNARE-complex inhibiting peptide blocks fusion of NR vesicles but preserves the fusion of vesicles in the initial RRP and RP

Analysis of the temporal kinetics of the different components of exocytosis does not explicitly provide information about the molecular state of the average vesicle in a vesicle pool. For example, a vesicle that is molecularly prepared for fusion but located at a distance from sites of Ca^{2+} entry would contribute to a late component of release relative to a molecularly prepared vesicle sitting at the Ca^{2+} channel cluster. Thus, we asked which of the three vesicle pools,

the RRP, the RP, and the NR, had already formed the SNARE complexes required for fusion and might thus be considered molecularly prepared for fusion. We probed for SNARE complex formation using a 23-amino-acid peptide termed "stx3pep" (Fig. 4 *A*) that mimics the N-terminal region of the SNARE binding domain of syntaxin3B, the specific syntaxin isoform expressed by retinal bipolar cells (39,55,56). Neuronal SNARE proteins are thought to assemble at the N-terminal half of the SNARE domain to a half-zippered SNARE complex that is required for the priming of synaptic vesicles (57,58). Therefore, we predicted that stx3pep would inhibit the formation of the syntaxin3B-containing SNARE complex. The control peptide, stx3con, contained the same 23 amino acids arranged in a different order (Fig. 4 *A*). We chose peptides over clostridial neurotoxins for this purpose because it is relatively straightforward to introduce peptides into a goldfish bipolar cell synaptic terminal via the recording electrode and because peptides function at room temperature (3,39,59,60), a physiologically relevant temperature for a nonmammalian vertebrate retinal neuron. To assess fusion competence, we measured stimulus-evoked changes in membrane capacitance.

First, we established the effects of the test peptide, stx3pep, and the control peptide, stx3con, on SNARE-complex formation in an in vitro assay. Neuronal SNAREs from brain extracts form an SDS-resistant complex in vitro that contain syntaxin 1, synaptobrevin, and SNAP-25 (61). This high-molecular-weight complex can be separated from the free SNARE proteins by SDS-PAGE electrophoresis. An equivalent high-molecular-weight SDS-resistant SNARE complex containing syntaxin3B was formed in vitro in retinal extract from goldfish retina (Fig. 4 *B*). However, addition of stx3pep significantly reduced the amount of syntaxin3 found in a high-molecular-weight, SDS-resistant SNARE complex when compared to stx3con or peptide-free control (Fig. 4 *B*, *top arrow*; Fig. 4 *C*). Concomitantly, in the presence of stx3pep there was an increase in free syntaxin3B that was not seen with stx3con or peptide-free conditions (Fig. 4 *B*, *bottom arrow*). These results, in combination with those of Curtis et al. (39), indicate that stx3pep, but not stx3con, blocks the formation of new ternary SNARE complexes required for exocytosis.

Fluorescein-tagged stx3pep or stx3con was introduced into an isolated bipolar cell synaptic terminal via the whole-terminal recording electrode. Peptide entry into the synaptic terminal was confirmed by observing the rise in synaptic fluorescein fluorescence. To control for potential differences in resting intraterminal Ca^{2+}, we once again employed a Ca^{2+}-buffered internal recording solution. Exocytosis from the different vesicle pools was evoked with our stimulus train and assayed by monitoring changes in membrane capacitance.

To probe the state of SNARE complex formation of the RRP, we compared the mean ΔC_{m1} in the presence of either

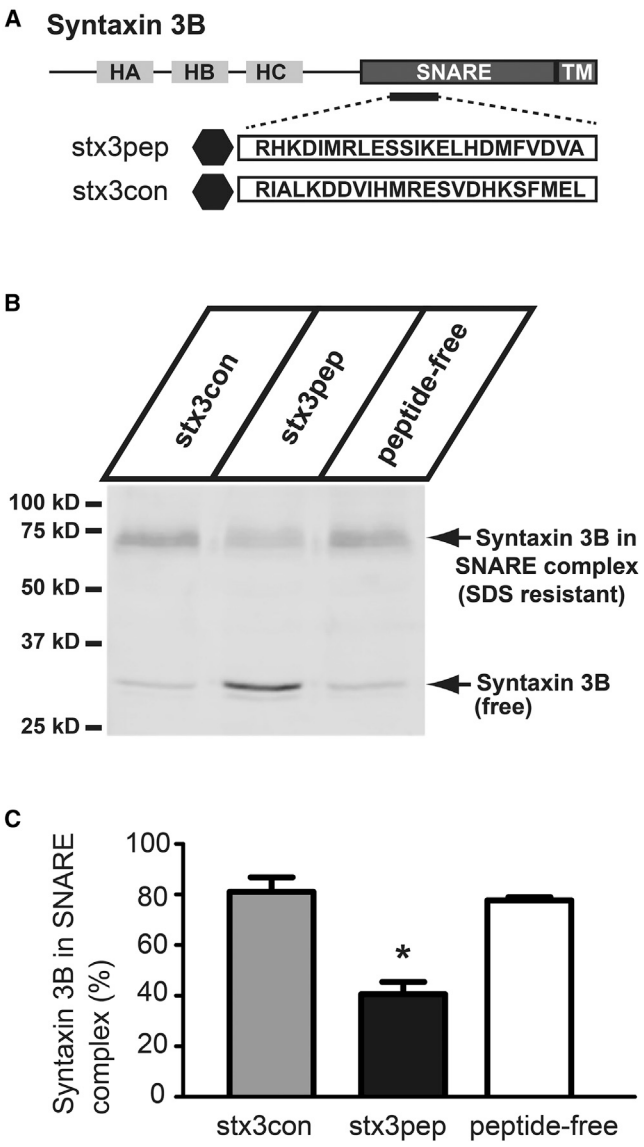

FIGURE 4 Stx3pep prevents the formation of SNARE complexes. (*A*) Domain model of syntaxin3B with the position and sequences of the SNARE domain peptide (stx3pep) and the scrambled control (stx3con). Location of the FITC label at the N-terminus of the peptides is depicted with a black hexagon. (*B*) A representative Western blot of goldfish retinal homogenate supernatant probed with an antibody specific for goldfish syntaxin3 (39). The blot reveals that in the presence of the control peptide stx3con or in the absence of added peptide (peptide-free), the majority of syntaxin3B was found in a high-molecular-weight SDS-resistant SNARE complex (*top arrow*). Stx3pep inhibited the formation of new SNARE complexes as evidenced by the increase in free syntaxin3B (*bottom arrow*) relative to control conditions. The remaining SNARE complexes (*top arrow*) were likely already assembled in the tissue before addition of stx3pep and were not affected by stx3pep. (*C*) Quantification of the high-molecular-weight SDS-resistant SNARE complex in the presence or absence of peptide. The amount of syntaxin3B present in the higher-molecular-weight SNARE complex relative to the total syntaxin3B is given. Stx3pep caused an ~50% reduction in the amount of syntaxin3B in the high-molecular-weight SNARE complex when compared to the control peptide stx3con or peptide-free control ($n = 2$, $p < 0.02$). Experiment was performed in duplicate using pooled extract prepared from four retinas.

stx3pep or stx3con 1 min after achieving the whole-terminal recording configuration. Stx3pep did not have a significant effect on ΔC_{m1} (Fig. 5 *A*; $p > 0.15$). However, to be certain that our sample size did not obscure a small inhibitory effect of stx3pep on the RRP, we conducted additional experiments in which an exocytosis was evoked by a single 20-ms depolarization given 1 min after break-in. We then pooled the secretory responses from the first 20-ms depolarization in the trains and the lone 20-ms depolarizations. The results, presented in Fig. 5 *B*, demonstrate that stx3pep did not reduce the magnitude of the RRP of ~30 fF, when compared to control terminals exposed to either stx3con or standard, peptide-free internal solution ($p > 0.9$). In addition, there was no evidence for a significant effect of either peptide on the presynaptic Ca^{2+} current (Fig. 5 *B*, *lower panel*; $p > 0.4$), consistent with a previous report indicating the lack of effect of this peptide on I_{Ca} (39).

We next considered the possibility that length of peptide exposure or peptide concentration, which took several minutes to reach a steady-state level within a terminal, might contribute to an inability to inhibit the initial RRP. To test this possibility, we increased the length of time from achieving the whole-terminal recording configuration to the first stimulus from 1 to 3 min. After 3 min of peptide exposure, stx3pep again failed to alter ΔC_{m1} relative to the control peptide stx3con or peptide-free control (Fig. 5 *B*, *blue bar*; $p > 0.4$), and once again, neither peptide altered the magnitude of the initial presynaptic Ca^{2+} current (Fig. 5 *B*, *lower panel*; $p > 0.4$). Thus, after several minutes of exposure to stx3pep, neither the initial RRP nor the initial I_{Ca} were altered in amplitude. These results, along with those of Fig. 3, suggest that RRP vesicles are molecularly prepared for rapid release with respect to both ATP-dependent preparatory steps (8,9) and SNARE complex formation.

In contrast to the inability of stx3pep to inhibit the initial RRP, stx3pep had a clear inhibitory effect on the total train-evoked capacitance response (Fig. 5 *A*). The mean ΔC_{mtotal} decreased from an average of >230 fF in control terminals to ~90 fF in the presence of stx3pep (Fig. 5 *C*, *upper panel*; $p < 0.02$), a reduction in exocytosis of >60%. The suppressive effect of stx3pep on total exocytosis was not readily attributable to altered Ca^{2+} entry (Fig. 5 *C*, *lower panel*, $p > 0.1$). Thus, the data indicate that ~150 fF's worth of new vesicles were recruited to the fusion-competent state during the stimulus train under standard conditions. The stx3pep-sensitive component of release (Fig. 5 *A*, *red curve*) suggests that this recruitment of new fusion-competent vesicles begins in earnest several seconds into the stimulus train, after RRP depletion.

The ~90 fF of exocytosis that was preserved in the presence of stx3pep was approximately three times larger than

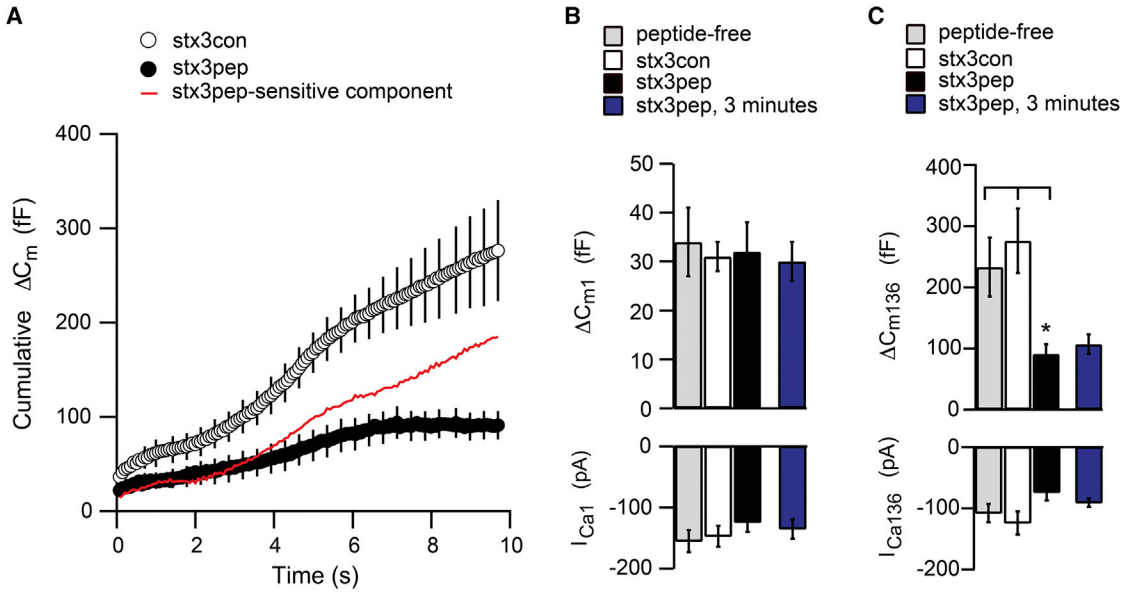

FIGURE 5 Stx3pep blocks the fusion of NR vesicles while preserving the ability of the initial the RRP and RP to fuse. (*A*) The capacitance records compare the mean cumulative rise in membrane capacitance over time in response to the stimulus train for stx3pep terminals (*solid circles*) and stx3con terminals (*open circles*). For ease of representation, error bars are displayed for every fifth data point. The difference trace (stx3con–stx3pep), representing the stx3pep-sensitive component of release, is shown in red. (*B*) Bar graphs compare the average magnitude of the capacitance response (*upper panel*) and Ca^{2+} current (*lower panel*) evoked by the first 20-ms depolarization (−60 to 0 mV) under peptide-free conditions (*gray bars*, $n = 12$), in the presence of stx3con (*open bars*, $n = 13$) or in the presence of stx3pep (*black bars*, $n = 13$). Shown in blue are the corresponding responses in stx3pep terminals when the first stimulus was given 3 min into the recording ($n = 9$). (*C*) Bar graphs compare the average magnitude of the total capacitance response (*upper panel*) and Ca^{2+} current (*lower panel*) under peptide-free conditions (*gray bars*, $n = 6$), in the presence of stx3con (*open bars*, $n = 5$) or in the presence of stx3pep (*black bars*, $n = 6$). Shown in blue are the corresponding responses in stx3pep terminals in which the stimulus train delayed until 3 min into the recording ($n = 9$).

could be accounted for by RRP vesicles alone. A similar result was observed when the peptide exposure time was tripled (Fig. 5 *C*). Clearly, numerous vesicles originating from outside of the RRP were insensitive to the inhibitory effects of stx3pep. Furthermore, the membrane capacitance in stx3pep terminals did not increase steadily throughout the stimulus train (Figs. 5 *A*). Rather, it reached a plateau approximately two-thirds of the way through the stimulus train, a pattern indicative of RP depletion (e.g., Fig. 2). Together with the results of Curtis et al. (39), these results establish that the initial RP is largely intact in the presence of stx3pep. Thus, many vesicles within the initial RP have apparently formed the SNARE complexes necessary to support stimulus-evoked exocytosis.

New SNARE complex formation is required for continuous stimulus-evoked release

If the suppression of total train-evoked release by stx3pep reflects inhibition of new SNARE complex formation required for ongoing release, then stx3pep should also inhibit the ability to refill the fusion-competent vesicle pools. To test the hypothesis that functional pool replenishment requires the formation of new SNARE complexes, terminals were dialyzed with either stx3pep or stx3con (e.g., Fig. 6 *A*, *solid* and *open bars*, respectively). Identical experiments, provided for comparison, were performed in a separate cohort of terminals dialyzed with standard, peptide-free intracellular solution (Figs. 6 and 7, *shaded markers*). One minute after achieving the whole-terminal recording configuration, the synaptic terminal was presented with multiple stimulus trains with an intertrain interval of 1 min until exocytosis ceased or a total of four trains were given.

Peptide-free and stx3con terminals exhibited a modest decrement in ΔC_{m1} across the four trains, indicating that there was significant refilling of the RRP between stimulus trains (Fig. 6). By contrast, there was a clear reduction in ΔC_{m1} in stx3pep terminals across the series of four stimulus trains compared to stx3con (Fig. 6). The inhibition by stx3pep relative to stx3con was significant by the second train (Fig. 6 *A*, $p < 0.03$; Fig. 6 *B*, $p < 0.02$). By the third train, half of the stx3pep terminals no longer exhibited a secretory response, whereas control terminals continued to respond robustly. By the fourth train, given 4 min into the recording, ΔC_{m1} was completely suppressed in the remaining stx3pep terminals (Fig. 6), whereas in stx3con or peptide-free terminals, ΔC_{m1} for the fourth train had a mean value of ~20 fF (Fig. 6 *A*). This inhibitory effect of stx3pep on replenishment of the RRP was activity-dependent, as in the absence of prior stimulation, the RRP remained fully intact for several minutes (Fig. 5 *B*). The inability to refill the ΔC_{m1} between trains in the presence of stx3pep is also evident from a difference in the slope of the relationship between the normalized ΔC_{m1} as a function of train number between stx3pep and stx3con (Fig. 6 *B*; $p < 0.001$) and the observation that total RRP release summed over the applied trains was significantly reduced in stx3pep terminals when compared to stx3con (Fig. 8 *A*, $p < 0.02$). A similar level of depression was observed when functional replenishment of synaptic vesicles was inhibited by ATP-γS (Fig. 8 *A*). The suppression of train-evoked exocytosis in the presence of stx3pep could not readily be accounted for by a difference in Ca^{2+} entry among conditions. I_{Ca1} for each train was not statistically different between groups, and the magnitude of I_{Ca1} was similar across trains (Fig. 6 *A*, *lower panel*).

With respect to the RP, stx3pep terminals also showed a clear decrement in ΔC_{mtotal} with each successive train when compared to control terminals (Fig. 7). For example, in response to the second stimulus train, ΔC_{mtotal} in the presence of stx3pep was ~40 fF, a value significantly different ($p < 0.011$) from the >130 fF response measured in the presence of stx3con (Fig. 7 *A*). This decrement is also evident in the mean normalized response evoked by the second stimulus train (Fig. 7 *B*, $p < 0.02$). Once again, half of the stx3pep terminals failed to mount a secretory response to the third train, in contrast to stx3con and peptide-free terminals. The total amount of exocytosis evoked by the fourth

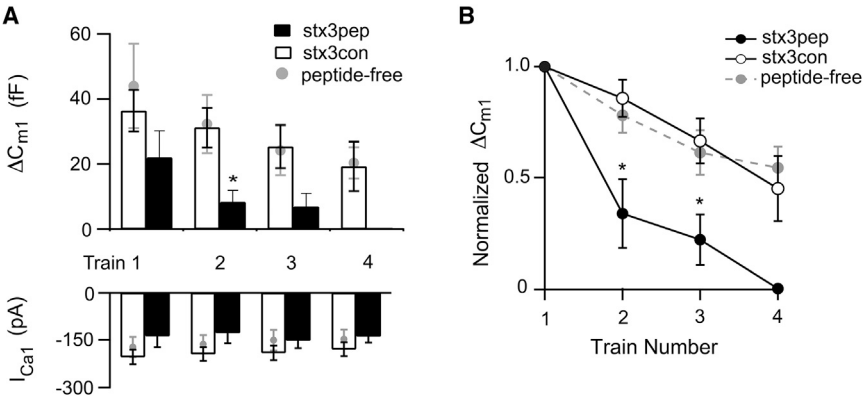

FIGURE 6 Stx3pep, but not stx3con, blocks refilling of the RRP. (*A*) Upper panel shows the average capacitance responses to the first depolarization (ΔC_{m1}) evoked by each of four stimulus trains given one minute apart. Synaptic terminals were dialyzed with internal solution containing either stx3pep (*solid bars*) or stx3con (*open bars*). In a separate cohort of experiments, provided for comparison purposes, terminals were dialyzed with standard, peptide-free internal solution (*shaded circles*). Lower panel gives the amplitudes of the corresponding Ca^{2+} currents. (*B*) ΔC_{m1} for trains 2–4 were normalized to the ΔC_{m1} obtained from train 1. The normalized ΔC_{m1} was plotted as a function of train number for each of the three treatment conditions: stx3pep (*solid circles*), stx3con (*open circles*) or peptide-free (*shaded circles*). For (*A*) and (*B*) stx3pep terminals: train, 1 $n = 6$; train 2, $n = 5$; trains 3–4, $n = 3$. For stx3con terminals, trains 1–2, $n = 5$; trains 3–4, $n = 4$. Peptide free terminals: trains 1, 2 $n = 6$, trains 3–4, $n = 5$.

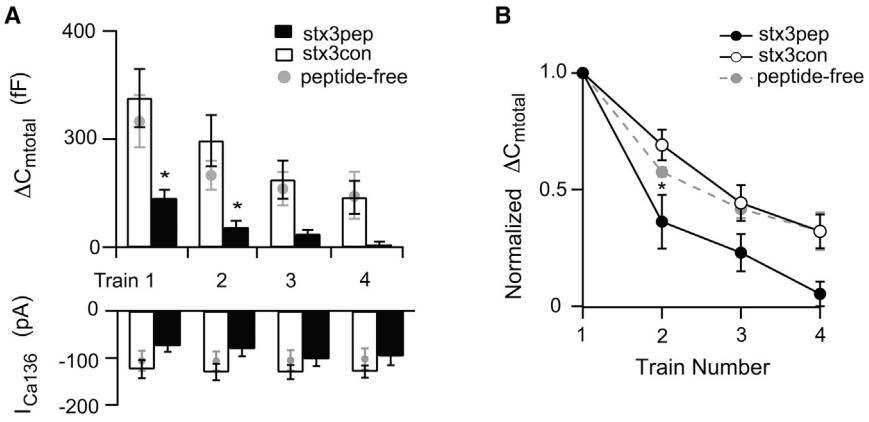

FIGURE 7 Stx3pep, but not stx3con, blocks refilling of the RP. (*A*) Upper panel shows the average capacitance responses to ΔC_{mtotal} evoked by each of four stimulus trains given one minute apart. Synaptic terminals were dialyzed with internal solution containing either stx3pep (*solid bars*) or stx3con (*open bars*). In a separate cohort of experiments, provided for comparison purposes, terminals were dialyzed with standard, peptide-free internal solution (*shaded circles*). Lower panel gives the amplitudes of the corresponding Ca^{2+} currents. (*B*) ΔC_{mtotal} for trains 2–4 were normalized to the ΔC_{mtotal} obtained from train 1. The normalized ΔC_{mtotal} was plotted as a function of train number for each of the three treatment conditions: stx3pep (*solid circles*), stx3con (*open circles*), or peptide-free (*shaded circles*). For (*A* and *B*) stx3pep terminals: train, 1 $n = 6$; train 2, $n = 5$; trains 3–4, $n = 3$. For stx3con terminals, trains 1–2, $n = 5$; trains 3–4, $n = 4$. Peptide-free terminals; trains 1, 2 $n = 6$; trains 3–4, $n = 5$.

train in the remaining stx3pep terminals averaged ~5 fF (Fig. 7 *A*), contrasting with the >90 fF responses observed in the presence of stx3con or peptide-free internal solution. The inability to refill the ΔC_{mtotal} between trains in the presence of stx3pep is also evident from a difference in the slope of the relationship between the normalized ΔC_{mtotal} as a function of train number between stx3pep and stx3con (Fig. 7 *B*; $p < 0.004$). The stx3pep-mediated inhibition of functional refilling of the RP was an activity-dependent effect, as evidenced by the fact that when the first train in stx3pep terminals was delayed several minutes, ΔC_{mtotal} was not suppressed (Fig. 5 *C*). The amplitudes of I_{Ca136} and I_{Ca1} in the presence of stx3pep were sufficient to drive exocytosis and did not decrement across trains more than those measured in the presence of stx3con or with peptide-free internal recording solutions (Fig. 7 *A*, *lower panel*).

To obtain an upper limit on the total number of vesicles in the primed state, as evidenced by either resistance to stx3pep or by a requirement for ATP hydrolysis (8,9), we quantified the total extent of release over the four stimulus trains in the absence of added peptide, in the presence of either stx3pep or stx3con, and when ATP-γS replaced ATP in the internal solution. Fig. 8 *B* demonstrates that in peptide-free conditions or in the presence of the control peptide stx3con, the average total cumulative ΔC_{mtotal} evoked over the four stimulus trains exceeded 500 fF. This is consistent with the ability to copiously recruit and subsequently fuse vesicles that did not initially reside in either the initial RRP or the initial RP. Compared to stx3con, stx3pep dramatically and significantly reduced the total cumulative ΔC_m from a mean value of ~700 to ~140 fF (Fig. 8 *B* $p < 0.005$), a level virtually identical to that obtained when functional pool refilling was prevented by ATP-γS (Fig. 8 *B* $p > 0.5$). Together, these data reveal that despite the ability to continuously release neurotransmitter and the large number of vesicles that fill the synaptic terminals of retinal bipolar cells, only ~150 fF's worth of vesicles had formed the SNARE complexes necessary for stimulus-evoked release.

Stx3pep inhibits the recruitment of new vesicles to the synaptic ribbons but not fusion of the ribbon-associated vesicle pools in the cone photoreceptor

Our results in the bipolar cell suggest that only RRP and RP vesicles, but not NR vesicles, are molecularly prepared for fusion. To test whether this may be true for other neurons that form ribbon-style synapses, we tested our peptides on neurotransmitter release from cone photoreceptors. Cone photoreceptors, like bipolar cells, express syntaxin3 (39,55,62). We recorded from pairs of synaptically coupled cone photoreceptors and horizontal cells in the retinal slice preparation (29). At the cone-horizontal cell synapse in salamander retina, postsynaptic currents (PSCs) are assembled from a linear sum of individual m-excitatory postsynaptic potentials (63,64), allowing us to use charge transfer as a measure of vesicle release. Integrating the total charge transfer of the horizontal cell PSC (Q_{PSC}) evoked by stimulation of a cone with the train yields a rapid increase in charge transfer reflecting synchronous release from the cone RRP followed by a second slower release of the RP (16,65) (Fig. 9 *A*). After ~1 s of stimulation under control conditions, the RP of vesicles on the ribbon is depleted and then charge transfer grows at a steady rate limited by the rate at which vesicles repopulate the ribbon (16,18,66).

After the achievement of simultaneous whole-cell recordings, we waited for 7 min to allow peptide to diffuse from the somatically positioned pipette into the cone photoreceptor terminal before giving the first stimulus train (42). We tested release from the initial RRP and RP by applying a 2-s train of pulses to −30 mV (25 ms pulses separated by 50-ms interpulse intervals, 13.3 Hz). This was immediately followed by a train of pulses to −10 mV for another 2 s. Increasing the pulse strength from −30 to −10 mV during

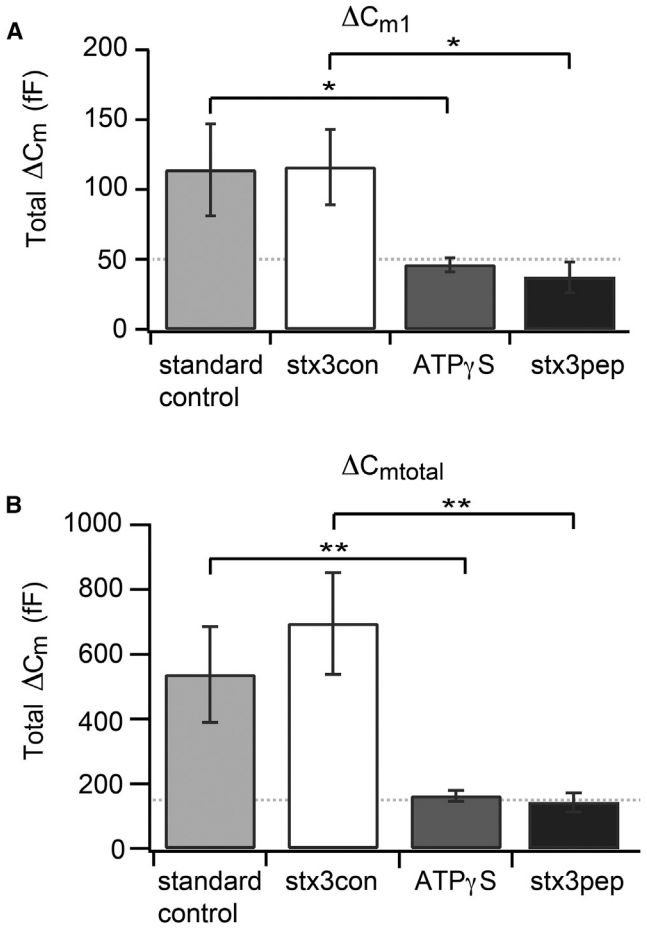

FIGURE 8 The maximum stimulus-evoked exocytosis in the presence of stx3pep is indicative of the RRP and the RP. (*A*) The total ΔC_{m1} evoked by the four stimulus trains exceeded 100 fF for terminals under standard control conditions or in the presence of the control peptide, stx3con. By contrast, total ΔC_{m1} was reduced in the presence of stx3pep ($p < 0.02$) and ATP-γS ($p \leq 0.05$) relative to their respective controls, stx3con, and standard control. Dotted line denotes 50 fF. (*B*) The cumulative total capacitance increase evoked by the stimulus trains, total ΔC_{mtotal} exceeded 500 fF under standard control conditions or in the presence of the control peptide stx3con. By contrast, total ΔC_{mtotal} was significantly reduced in the presence of either stx3pep ($p < 0.004$) or ATP-γS ($p < 0.002$) relative to their respective controls, stx3con and standard control. Dotted line denotes 150 fF. Standard control terminals ($n = 6$), ATP-γS terminals ($n = 6$), stx3pep terminals ($n = 6$), and stx3con terminals ($n = 5$).

the train increases Ca^{2+} influx and has been shown to cause a Ca^{2+}-dependent acceleration of vesicle replenishment to the synaptic ribbons (18,42).

The amplitude of the PSC evoked by the initial step to −30 mV was similar between stx3pep and stx3con cone photoreceptors (Fig. 9 *C*, *left*; stx3con: 50.28 ± 10.46 pA, $n = 14$; stx3pep: 55.78 ± 12.02 pA, $n = 9$; $p > 0.7$, unpaired *t*-test). This test pulse releases ~60% of the RRP (65) and so this result indicates that the RRP was not significantly affected by stx3pep. With a maintained train of pulses, the entire RRP and RP are both ultimately released. To measure the combined size of the RRP and RP, we fit the rise in charge transfer with a single exponential and found it too was similar in stx3pep and stx3con cones (Fig. 9 *C*, *right*; stx3con: 1.81 ± 0.37 pC; stx3pep: 1.892 ± 0.36 pC, $p = 0.89$, unpaired *t*-test). The limiting slope of the increase in charge transfer during the train of pulses −30 mV, which reflects the rate at which vesicles replenish the ribbon and is driven largely by the number of available release sites on the ribbon (65,67), also did not differ between the two conditions (Fig. 9 *D*; stx3con: −1.225 ± 0.2033 pC/s, $n = 14$; stx3pep: −1.275 ± 0.1652 pC/s, $n = 9$; $p > 0.8$). In the presence of stx3con, this limiting slope increased significantly when the pulse strength was increased to −10 mV ($p \leq 0.002$, paired *t*-test) reflecting the Ca^{2+}-dependent acceleration of vesicle replenishment to ribbons (18,66). By contrast, in the presence stx3pep, the rate of charge transfer did not increase significantly after increasing pulse strength to −10 mV ($p > 0.1$). This finding suggests that stx3pep inhibited the Ca^{2+}-dependent recruitment of new vesicles to the synaptic ribbons and/or their subsequent fusion. Measurements of charge transfer are quite sensitive to subtraction of the spontaneous background release measured in each trial before the pulse train. To minimize this source of trial-to-trial variability, we additionally compared the change in slope within trials caused by the increase in pulse train strength from −30 to −10 mV. Results show that the acceleration of release was significantly diminished in stx3pep cones relative to stx3con cones (Fig. 9 *E*; $p \leq 0.022$). Together, these data indicate that in cone photoreceptors, stx3pep has little effect on the fusion of initial RRP or RP vesicles, whereas stx3pep inhibited the fusion of vesicles newly recruited to the synaptic ribbons.

DISCUSSION

The RP is located at the ribbon-style active zone and replenishes the RRP

The ability of the RRP to cross-deplete the RP demonstrates a functional relationship between these two vesicle populations (Fig. 3). A functional relationship could be explained by the sharing of an essential, limited resource for exocytosis, the leading candidates for which are synaptic vesicles and/or fusion sites that have undergone all the ATP-dependent preparatory steps necessary for fusion (9,33,48). Either would require that the two pools be in close physical proximity, and this is supported by our cross-depletion experiments. Each 20-ms depolarization generated a brief, local elevation of intraterminal Ca^{2+} that was sufficient to drive RRP depletion without inducing a measurable change in the spatially averaged intraterminal Ca^{2+} (data not shown), consistent with previous studies indicating that these kinds of stimuli generate a brief, microdomain of elevated Ca^{2+} (19,54,68). The spacing between each 20-ms depolarization exceeded the time required for Ca^{2+} microdomain collapse by approximately three orders of magnitude (54), and

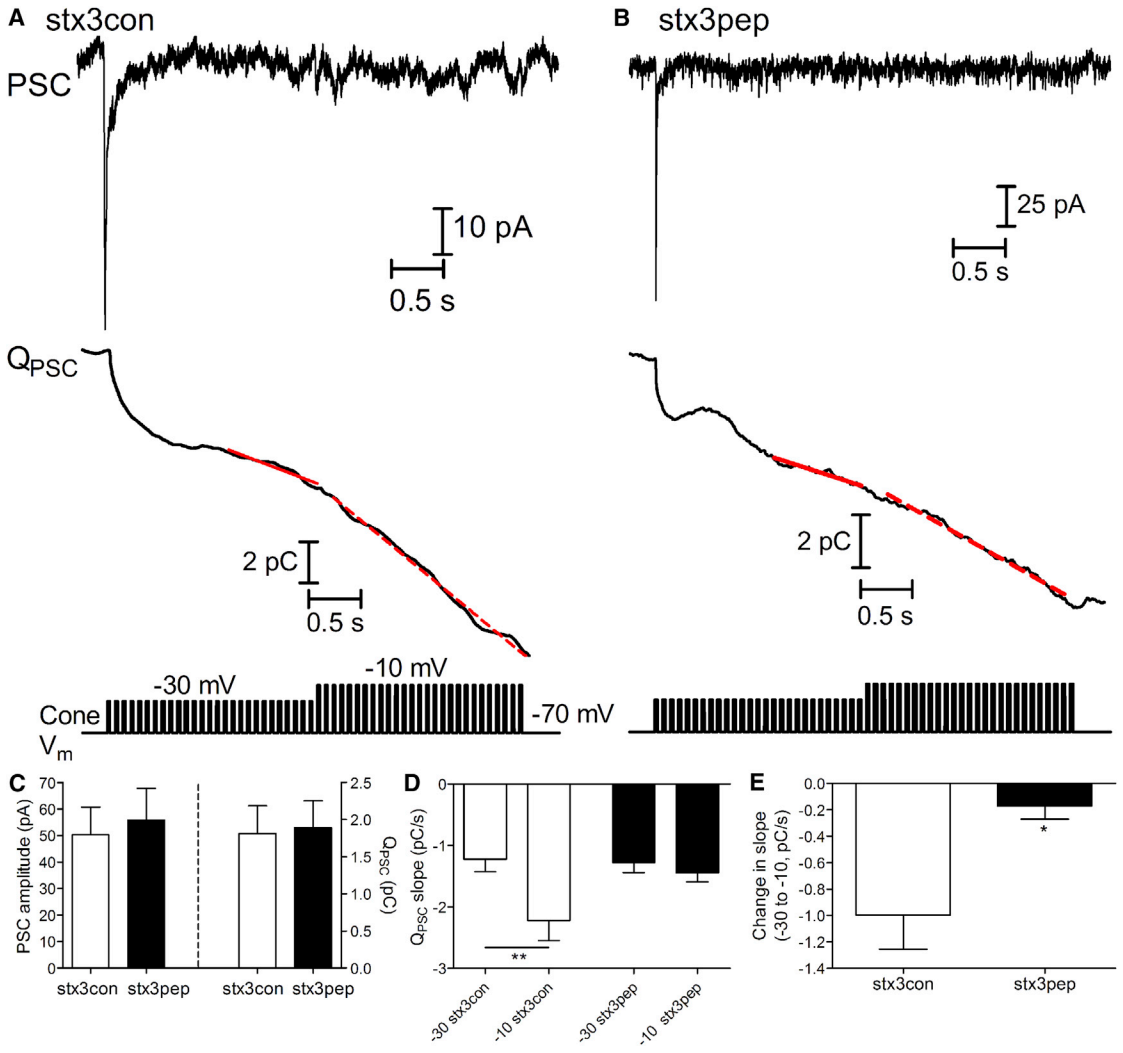

FIGURE 9 Stx3pep inhibits the fusion of vesicles newly arrived to the synaptic ribbons. (*A*) Upper trace shows a representative set of PSCs evoked in a voltage-clamped horizontal cell by a pulse train voltage protocol, depicted in the lower trace, applied to a simultaneously voltage-clamped cone after introduction of stx3con. After correcting for spontaneous release from neighboring photoreceptors (Methods), PSCs were integrated to show the cumulative charge transfer (Q_{PSC}) evoked by the pulse train voltage protocol (*middle trace*). The rate of replenishment during the train of pulses to −30 mV was assessed by fitting the limiting slope during the final 1 s of the first phase of the pulse train (*solid red line* at *left*; slope = −1.924 pC/s). The rate of replenishment during the train of pulses to −10 mV was assessed from the slope of the line fit to the final 1.8 s of that train (*dashed red line*; −4.170 pC/s). (*B*) Representative PSC evoked by the same train protocol in a cone-horizontal cell pair after introduction of stx3pep shows a smaller change in the limiting slope of PSC charge transfer after switching from the −30 mV train of pulses (−1.262 pC/s) to the −10 mV train (−2.214 pC/s). (*C*) (*Left*) Amplitude of the initial PSCs evoked by the first pulse to −30 mV during the trains did not differ significantly in recordings with the stx3pep or stx3con ($p < 0.7$, unpaired *t*-test). (*Right*) The rise in charge transfer did not differ significantly in recordings with the stx3pep or stx3con ($p > 0.8$, unpaired *t*-test). (*D*) In the presence of stx3con, the slope increased significantly when pulse strength was increased to −10 mV (slope, −2.223 ± 0.3232 pC/s, $n = 14$; $^{**}p \leq 0.002$, paired *t*-test). With stx3pep, the slope did not increase significantly after increasing pulse strength to −10 mV (slope: −1.448 ± 0.1453 pC/s, $n = 9$; $p > 0.1$). (*E*) The change in slope within trials produced by increasing the pulse from −30 to −10 mV was significantly greater with stx3con (−0.9977 ± 0.2585 pC/s, $n = 14$) than with stx3pep (−0.1728 ± 0.09919 pC/s, $n = 9$; $^{*}p \leq 0.022$, unpaired *t*-test).

there was no evidence of a rise in the spatially averaged intraterminal Ca^{2+} concentration as a consequence of the sequence of 20-ms depolarizing pulses (Fig. 3 *A*). In addition, there was no evidence of Ca^{2+}-dependent Ca^{2+} channel inactivation during a 20-ms depolarization (69) or as a consequence of the sequence of 20-ms depolarizations (Fig. 3 *B*). Thus, it seems unlikely that at sites distant from the voltage-gated Ca^{2+} channels, the intraterminal Ca^{2+} concentration reached the concentrations necessary to drive RP release (8,19,20,68) or delayed asynchronous release (25). Rather, the data are most consistent with a location for the RRP and RP within a Ca^{2+} microdomain at the ribbon-style active zones.

In a model of synaptic ribbon function initially proposed by Bunt (70), fusion of the synaptic vesicles with the plasma membrane during exocytosis occurs at the base of the synaptic ribbon, and the supply of vesicles to the ribbon base is supported by the downward movement of vesicles located

at the higher rows of the synaptic ribbons to the ribbon bases (1,2,5,53,71). According to this model, the RRP of the goldfish bipolar cell would be refilled approximately four times in the absence of functional replenishment of the ribbon-associated vesicles because each synaptic ribbon tethers approximately five rows of synaptic vesicles (2,24). Thus, a tantalizing explanation for the results of the cross-depletion experiment depicted in Fig. 3 is that the four to five rounds of RRP release correspond to the fusion of vesicles initially residing in the RRP vesicles, followed by the refilling of the RRP from vesicles originating in the upper rows of the synaptic ribbon and their subsequent stimulus-evoked fusion. Direct support for this interpretation comes from a recent study in which individual synaptic vesicles located at a membrane-distal location on the synaptic ribbon were observed to progress in a membrane-proximal direction in response to an RRP-depleting stimulus (72,73). This explanation is also consistent with a requirement for functional synaptic ribbons for RP release (5,22). Models of vesicle fusion at synaptic ribbons model will be discussed in more detail in a subsequent section.

Finally, we note that the cross-depletion of the RP by the RRP in the bipolar cell synaptic terminal was not complete (Fig. 3, *C* and *D*). The residual ~14 fF secretory response could reflect ectopic release. However, the complete blockade of functional RP replenishment by ATP-γS typically requires more than one round of RP turnover, and this is the case even when exocytosis is triggered in a manner expected to drive the fusion of all primed synaptic vesicles situated at the plasma membrane, including those at ectopic sites (8,9). Thus, it is conceivable that the residual release after cross-depletion contains contributions caused by the incomplete blockade of functional replenishment by ATP-γS. This incomplete blockade could arise from the production of endogenous ATP, which was not inhibited in our experiments (8,9). Therefore, we suggest that the residual ~14 fF response be regarded as an upper limit on ectopic release, contributing at most, 20% of the RP. This interpretation agrees well with recent studies suggesting that 80% or more of the fast and slow components of neurotransmitter release, reflecting exocytosis respectively from the RRP and RP, requires functional synaptic ribbons (5,22).

The RRP and the RP have formed the SNARE complexes required for exocytosis

The rate with which vesicles fuse in response to a stimulus is often taken as an indication of whether or not vesicles are primed. Here, we used a peptide that interferes with new SNARE complex formation, stx3pep, to determine whether or not vesicles in a particular vesicle pool are primed. We found that the fusion of vesicles in the RRP of bipolar synaptic terminals and cone photoreceptors was not affected by stx3pep (Figs. 5, 6, and 9, *A* and *C*). Furthermore, in the absence of stimulus-evoked vesicle turnover, the magnitude of the RRP was stable on a timescale of several minutes or more (e.g., Fig. 5). The RRP was also capable of stimulus-evoked fusion in the presence of ATP-γS (Figs. 2, 3, and 8 *A*), indicating that the RRP or its associated release sites, have undergone all the ATP-dependent preparatory steps required for fusion, one of which is the dissolution of post-fusion SNARE complexes and the regeneration of available SNARE protein binding partners (74,75). A straightforward interpretation of these findings is that vesicles in the initial RRP of bipolar cells and photoreceptors have already formed the SNARE complexes necessary for membrane fusion and are thus, molecularly primed for fast, Ca^{2+}-triggered release. Paired with positional-priming (76,77), molecular priming of the RRP renders these vesicles capable of rapid fusion in response to activation of voltage-gated Ca^{2+} channels.

Our results indicate that the RP is also molecularly primed, despite the fact that it is not positionally primed (78). The SNARE complex-inhibiting peptide stx3pep failed to impede fusion of the RP in bipolar cell synaptic terminals (Figs. 5 and 8 *B*) and in cone photoreceptors (Fig. 9). The former agrees well with an earlier study in which stx3pep failed to inhibit the first round of RP release evoked by a single depolarizing voltage step, although it inhibited subsequent rounds of release (39). As observed for the RRP, in the absence of stimulation, the magnitude of the bipolar cell RP was stable over a timescale of minutes or more (Fig. 5 *C*), suggesting that the effect of stx3pep on subsequent release events required the turnover of synaptic vesicles and/or release sites. The initial bipolar cell RP was also able to fuse in the absence of ATP-hydrolysis (Figs. 2 and 8), in agreement with previous studies indicating that the RP or its associated release sites have passed through all the ATP-dependent preparatory steps required for fusion (8,9,33).

A molecularly primed RP that is not positionally primed is an attractive interpretation that can account for the perplexing finding that bipolar cell RP vesicles are capable of fusing at the same rate as RRP vesicles when triggered by the rapid, global elevation of Ca^{2+} but not when evoked by membrane depolarization (8,14,68). However, it is also a somewhat surprising result that warrants further discussion. One important consideration is whether peptides are able to access the synaptic ribbon area. Fluorescently tagged RIBEYE peptides, some of which are double the length of stx3pep, effectively label the synaptic ribbons of living bipolar cells and photoreceptors (5,16,59,79,80). Moreover, RIBEYE peptides are typically introduced via a patch pipette and would thus face similar diffusional barriers as the peptides in this study. Thus, it seems that peptides are not restricted from accessing the synaptic ribbon area in either bipolar cells or photoreceptors. Stx3pep was active inside living cells, as it inhibited the fusion of NR vesicles in both bipolar cell synaptic terminals and cone photoreceptors and the replenishment of the RRP and RP (Figs. 5, 7, 8, and 9). This effect was specific, as evidenced by the fact that our control peptide did not alter any aspect of exocytosis,

and RIBEYE peptides, which clearly access the ribbon-style active zones, do not block exocytosis in their native state (3,80). Changes in release observed in the presence of stx3pep were not an artifact of how we quantified exocytosis, as two different approaches were used, membrane capacitance measurements and paired-recordings, and these yielded similar results in bipolar cell terminals and cone photoreceptors, respectively. Finally, we have observed similar effects on bipolar cell exocytosis in the presence of a different SNARE domain peptide. This peptide, based upon SNAP-25, also prevented the recruitment of new vesicles to the fusion competent state while sparing fusion of the initial RRP and RP (Fig. S1).

Continuous neurotransmitter release requires the recruitment of new vesicles to the fusion-competent state

A hallmark of ribbon-style synapses is their ability to continuously relay visual information to downstream neurons (1). Our results suggest that the recruitment of new vesicles to the molecularly primed state is essential for this ability. In bipolar cell terminals, both ATP-γS and stx3pep blocked a late component of release that was essential for sustaining exocytosis over a period of seconds (e.g., Figs. 2, 5, and 8). This important finding indicates that this later component of release is not delayed in its ability to contribute to the secretory response simply because it originates at sites distant from the sites of Ca^{2+} entry. Rather, these vesicles are not initially in a molecular state that supports fusion. The data also provide a molecular-level explanation for why the many synaptic vesicles in a bipolar cell synaptic terminal near the plasma membrane but outside of the RRP or RP fail to fuse in response to the global elevation of intraterminal Ca^{2+} (8,68); they are not molecularly primed. Although the NR component may contain contributions from the fusion of ectopic vesicles, this component of release became prominent after RRP depletion (Fig. 5 *A*), and its presence is correlated with the ability to replenish the RRP and RP (Figs. 5, 6, 7, and 8). These observations suggest a role for NR vesicles in the replenishment of the ribbon-associated vesicle pool. Consistent with this interpretation, stx3pep blocked a component of neurotransmitter release in cone photoreceptors that has been shown previously to correspond to the Ca^{2+}-accelerated, calmodulin-dependent recruitment of synaptic vesicles to the synaptic ribbons, followed by their subsequent fusion (Fig. 9) (18,66). Together our data indicate that new SNARE formation is critical for maintaining the supply of fusion-competent vesicles at synaptic ribbons.

Vesicles on the synaptic ribbons form intervesicular SNARE complexes

More than 45 years have passed since Bunt proposed that synaptic vesicles move along the synaptic ribbons in a conveyor-belt-like fashion to the plasma membrane, where they release their contents (70). Although numerous modifications of that initial model have been suggested since then, ribbon-style active zones remain enigmatic (1,53,71–73,81). Three models of vesicle fusion at ribbon-style active zones compatible with the main findings of this study are discussed below (Fig. 10).

In Model 1, there is a finite number of fusion sites on the plasma membrane at the ribbon-style active zones where vesicles can fuse (Fig. 10 *A*). Vesicles on the synaptic ribbon, in addition to the occasional vesicle from the cytoplasmic reserve, avail themselves of these fusion sites. An implication of this model is that it is the number of prepared fusion sites not vesicles that determines the magnitude of the secretory response. Model 1 would allow for cross-depletion of the RP by the RRP, as the vesicles would compete for the limited number of fusion sites. Model 1 must also account for the lack of an effect of stx3pep on RP vesicle fusion. One way it could do this would be to form t-SNARE receptor complexes between syntaxin and SNAP-25. These would await the arrival of a vesicle and the subsequent formation of the ternary SNARE complexes with vesicular synaptobrevin that are required for fusion. This is an attractive possibility, however evidence from in vitro reconstitution experiments suggest that syntaxin and SNAP-25 do not form stable t-SNARE receptors, but instead form complexes among themselves that are not part of the fusion pathway (82,83). Whether this is also true within the native, presynaptic environment remains to be determined.

In Model 2, there is also a finite number of fusion sites on the plasma membrane in the vicinity of the ribbon-style active zones; however, these sites are not vacant, but rapidly occupied by vesicles (Fig. 10 *B*). Vesicles at these plasma membrane sites define the RRP and the RP. Model 2 also requires a mechanism that sets the magnitude of the RP. Such a mechanism is unlikely to come from a limitation in vesicle number, as vesicles are highly abundant in synaptic endings that form ribbon-style synapses. The availability of syntaxin to form SNARE complexes could be one factor that governs the number of fusion sites. Syntaxin has two major conformational states. In the closed-state, syntaxin does not readily interact with SNARE-binding partners and cannot form SNARE complexes, whereas in the open or activated state, it does (84,85). Syntaxin typically requires Munc13 for its activation (83,86), but this may not be true of retinal ribbon-style synapses, as Munc13 does not appear to be required for photoreceptor exocytosis (87). Moreover, retinal ribbon-style synapses express an unusual isoform of syntaxin, syntaxin3B (39,56) that may have an alternate activation mechanism. Phosphorylation of syntaxin3B at Thr^{14} facilitates its interaction with SNAP-25, and Ca^{2+}-calmodulin-dependent protein kinase II phosphorylates this site in vitro (88). This raises the possibility that syntaxin3B may be activated in a Ca^{2+}-dependent

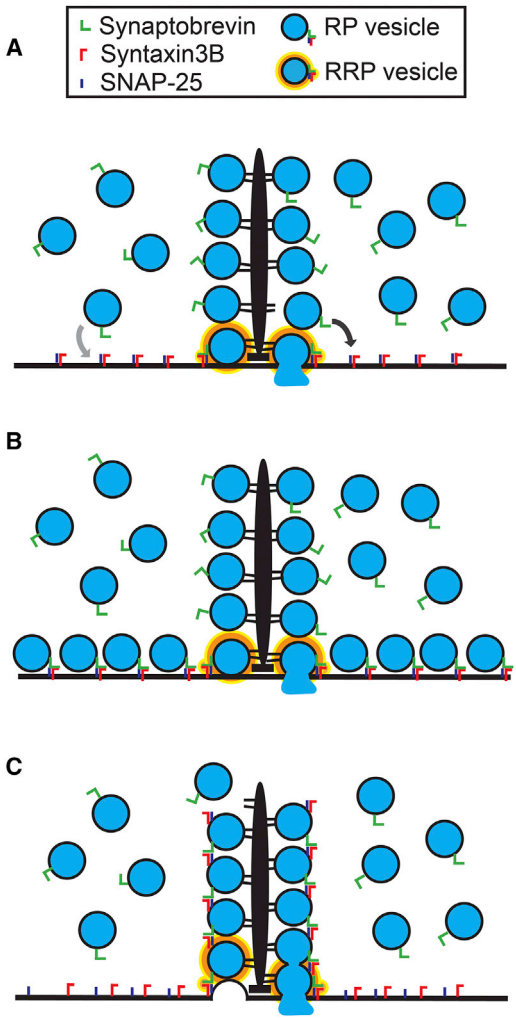

FIGURE 10 Three models of vesicle fusion at retinal ribbon-style synapses. (*A*) In Model 1, there is a finite number of t-SNARE receptor complexes on the plasma membrane that are formed between syntaxin3B and SNAP-25 at the ribbon-style active zone. Vesicles on the synaptic ribbon (e.g., *black arrow*), in addition to the occasional vesicle from the cytoplasmic reserve (e.g., *gray arrow*), avail themselves of these fusion sites to form the RP. The RRP is comprised of those vesicles that form SNARE complexes at the ribbon bases, where the Ca^{2+} channels cluster. (*B*) In Model 2, SNARE complexes are formed between synaptobrevin on synaptic vesicles and the t-SNAREs syntaxin3B and SNAP-25 that are located on the plasma membrane at the ribbon-style active zone. Both the RRP and the RP reside on the plasma membrane. (*C*) In Model 3, vesicles on the synaptic ribbon form intervesicular SNARE complexes. Vesicles at the ribbon bases additionally form SNARE complexes with plasma membrane t-SNAREs. Vesicles can fuse individually, as shown on the left side of the ribbon, or via compound fusion, as shown on the right side of the ribbon. For all, synaptic ribbons, vesicle tethers and plasma membrane are shown in black. Synaptic vesicles (*blue*) contain synaptobrevin (*green*). Syntaxin3B (*red*) and SNAP-25 (*dark blue*) are found on the plasma membrane (*A–C*) and in low numbers on the synaptic vesicle membranes, but vesicular syntaxin3B and vesicular SNAP-25 are depicted only when they participate in intervesicular SNARE complexes (*C*). Fusion-competent vesicles (RP and RRP) are denoted by the presence of a SNARE complex. RRP vesicles are additionally outlined in orange.

manner. This type of mechanism could restrict the formation of functional SNARE complexes to regions of elevated Ca^{2+}, such as are found at ribbon-style active zones (51,54), setting a limit on the number of available fusion sites. Model 2 would provide an explanation for why the kinetics of RP release evoked by the flash-photolysis of caged Ca^{2+} in bipolar cell synaptic terminals is indistinguishable from that of the RRP, but is slower in response to the activation of voltage-gated channels (8,14,19,68). However, as the vesicles in each pool form their own SNARE complexes with the plasma membrane, Model 2 does not readily account for the cross-depletion of the RP by the RRP. Nor is it evident from this model why exocytosis from the RRP or the RP would require functional synaptic ribbons (5,22), although changes in the active zone protein complex after ribbon inactivation or ribbon loss may help explain some of that requirement (89).

In Model 3, the RP is defined as the ribbon-tethered vesicle pool (Fig. 10 *C*). These RP vesicles have formed the SNARE complexes necessary for Ca^{2+}-evoked exocytosis. However, as only the bottom rows of vesicles, the RRP, form SNARE complexes with the plasma membrane, the other RP vesicles make intervesicular SNARE complexes formed by the interaction of cognate SNAREs on neighboring synaptic vesicles. In support of this hypothesis, we note that syntaxin and SNAP-25 are both found on synaptic vesicle membranes, albeit at relatively low levels (90). However, only a few SNARE complexes are required to catalyze fusion (91–93), and the formation of these complexes may be aided by the tight-packing of the vesicles that are tethered to synaptic ribbons (2,9,23). Furthermore, there is precedent for syntaxin3, utilized by ribbon-style synapses (39,55,56), to play a role in intervesicular fusion. In mast cells, syntaxin3 has been localized to secretory granules, where it may mediate compound fusion, a known feature of mast cell exocytosis (94–96) (unpublished data, E. Sanchez-Goray, R. H., and R. Adachi).

Model 3 supports the fusion of an individual RRP vesicle with the plasma membrane (Fig. 10 *C*, *left side of ribbon*) or a wave of fusion that spreads up the synaptic ribbon (Fig. 10 *C*, *right side of ribbon*) (1,71). It would also explain the ability of the RP to fuse with identical kinetics as the RRP in response to flash-photolysis of caged-Ca^{2+}, but not in response to activation of voltage-gated Ca^{2+} channels, and it would allow for cross-depletion of the RP by the RRP. In addition, the invocation of intravesicular fusion could help explain changes in active zone morphology that occur with strong stimulation. These include the apparent movement of membrane up along the synaptic ribbon with stimulation, which was originally interpreted as the movement of the ribbon into the plasma membrane, but could instead indicate a wave of fusion up the ribbon (1,71,97), and the discovery of larger structures attached to the synaptic ribbons of stimulated bipolar cell synaptic terminals that have the appearance of several vesicles fused together (33).

Model 3 also allows for the possibility of multivesicular release, a feature of many neurons including those that form ribbon-style synapses (12,98,99), one form of which may arise from the fusion of vesicles with each other before fusion with the plasma membrane (1,71). In addition, Model 3 provides a molecular rationale for the recent demonstration that exocytosis in retinal bipolar cells is not restricted to those vesicles located at the ribbon bases and in contact with the plasma membrane, but also occurs at sites along the synaptic ribbon that are distant from the plasma membrane (73). Finally, we note that although Model 3 is most consistent with available data, each of these models represents only a snapshot in time. The preferred mode of release may be dynamically regulated and depend on factors not examined here, such as the molecular environment or local Ca^{2+} signals.

CONCLUSIONS

The results of this study provide evidence that at the ribbon-style synapses of bipolar cells and cone photoreceptors, there are two vesicle pools that have formed the SNARE complexes required for Ca^{2+}-evoked exocytosis. Both pools are likely to be associated with the synaptic ribbons, and the synaptic ribbon emerges as a site of SNARE-dependent priming, adding to previous suggestions that the synaptic ribbons serve as a site of ATP-dependent preparation for fusion. Vesicles tethered to the synaptic ribbon may form intervesicular SNARE complexes, while those located at the ribbon bases and contact the plasma membrane form SNARE complexes with the plasma membrane. RP vesicles can replenish the RRP. This may occur via the downward movement of vesicles on a ribbon or by a wave of fusion that sweeps up the ribbon, the choice of which may ultimately depend upon the interplay between factors such as the stimulus-evoked Ca^{2+} signal, endocytosis, and the activation of syntaxin3B. New SNARE complex formation is critical for maintaining the supply of fusion-competent vesicles at synaptic ribbons and the ability to maintain continuous, stimulus-evoked release. Other components of neurotransmitter release have been described in neurons that form ribbon-style synapses that are more loosely coupled to Ca^{2+} entry through voltage-gated Ca^{2+} channels than those examined here. Important goals for the future are to determine the extent to which vesicles participating in these additional components of release are initially fusion competent and to identify those mechanisms that recruit vesicles to the fusion-competent state at ribbon- and nonribbon release sites.

SUPPORTING MATERIAL

One figure is available at http://www.biophysj.org/biophysj/supplemental/S0006-3495(17)30871-8.

AUTHOR CONTRIBUTIONS

R.H., P.D., W.B.T., and R.J. designed the research. All authors participated in the collection and analysis of data. P.D. and R.H. wrote the manuscript.

ACKNOWLEDGMENTS

We thank Dr. Alice Chuang for help with statistical methods, Natalia Bogdanova and Dr. Xiaoqin Liu for technical assistance, and Dr. M. Neal Waxham for assistance with peptide quantification.

This work was supported by awards from the National Eye Institute of the National Institutes of Health to R.H. (EY012128) and W.B.T. (EY10542), and a Senior Scientific Investigator Award from Research to Prevent Blindness (to W.B.T.). Additional support from a Sam Taub and Beatrice Burton Endowed Fellowship in Vision Disease (to P.D.) is gratefully acknowledged.

REFERENCES

1. Heidelberger, R., W. B. Thoreson, and P. Witkovsky. 2005. Synaptic transmission at retinal ribbon synapses. *Prog. Retin. Eye Res.* 24:682–720.
2. Sterling, P., and G. Matthews. 2005. Structure and function of ribbon synapses. *Trends Neurosci.* 28:20–29.
3. Zenisek, D. 2008. Vesicle association and exocytosis at ribbon and extraribbon sites in retinal bipolar cell presynaptic terminals. *Proc. Natl. Acad. Sci. USA.* 105:4922–4927.
4. Chen, M., M. J. Van Hook, …, W. B. Thoreson. 2013. Properties of ribbon and non-ribbon release from rod photoreceptors revealed by visualizing individual synaptic vesicles. *J. Neurosci.* 33:2071–2086.
5. Snellman, J., B. Mehta, …, D. Zenisek. 2011. Acute destruction of the synaptic ribbon reveals a role for the ribbon in vesicle priming. *Nat. Neurosci.* 14:1135–1141.
6. Midorikawa, M., Y. Tsukamoto, …, M. Tachibana. 2007. Different roles of ribbon-associated and ribbon-free active zones in retinal bipolar cells. *Nat. Neurosci.* 10:1268–1276.
7. Zampighi, G. A., C. Schietroma, …, N. C. Brecha. 2011. Conical tomography of a ribbon synapse: structural evidence for vesicle fusion. *PLoS One.* 6:e16944.
8. Heidelberger, R. 1998. Adenosine triphosphate and the late steps in calcium-dependent exocytosis at a ribbon synapse. *J. Gen. Physiol.* 111:225–241.
9. Heidelberger, R., P. Sterling, and G. Matthews. 2002. Roles of ATP in depletion and replenishment of the releasable pool of synaptic vesicles. *J. Neurophysiol.* 88:98–106.
10. Wan, Q. F., and R. Heidelberger. 2011. Synaptic release at mammalian bipolar cell terminals. *Vis. Neurosci.* 28:109–119.
11. Heidelberger, R. 2001. Electrophysiological approaches to the study of neuronal exocytosis and synaptic vesicle dynamics. *Rev. Physiol. Biochem. Pharmacol.* 143:1–80.
12. Kim, M. H., G. L. Li, and H. von Gersdorff. 2013. Single Ca^{2+} channels and exocytosis at sensory synapses. *J. Physiol.* 591:3167–3178.
13. Jarsky, T., M. Tian, and J. H. Singer. 2010. Nanodomain control of exocytosis is responsible for the signaling capability of a retinal ribbon synapse. *J. Neurosci.* 30:11885–11895.
14. Mennerick, S., and G. Matthews. 1996. Ultrafast exocytosis elicited by calcium current in synaptic terminals of retinal bipolar neurons. *Neuron.* 17:1241–1249.
15. Palmer, M. J. 2010. Characterisation of bipolar cell synaptic transmission in goldfish retina using paired recordings. *J. Physiol.* 588:1489–1498.
16. Bartoletti, T. M., N. Babai, and W. B. Thoreson. 2010. Vesicle pool size at the salamander cone ribbon synapse. *J. Neurophysiol.* 103:419–423.

17. Sakaba, T., M. Tachibana, …, N. Minami. 1997. Two components of transmitter release in retinal bipolar cells: exocytosis and mobilization of synaptic vesicles. *Neurosci. Res.* 27:357–370.
18. Babai, N., T. M. Bartoletti, and W. B. Thoreson. 2010. Calcium regulates vesicle replenishment at the cone ribbon synapse. *J. Neurosci.* 30:15866–15877.
19. von Gersdorff, H., and G. Matthews. 1994. Dynamics of synaptic vesicle fusion and membrane retrieval in synaptic terminals. *Nature.* 367:735–739.
20. von Gersdorff, H., T. Sakaba, …, M. Tachibana. 1998. Submillisecond kinetics of glutamate release from a sensory synapse. *Neuron.* 21:1177–1188.
21. Innocenti, B., and R. Heidelberger. 2008. Mechanisms contributing to tonic release at the cone photoreceptor ribbon synapse. *J. Neurophysiol.* 99:25–36.
22. Maxeiner, S., F. Luo, …, T. C. Südhof. 2016. How to make a synaptic ribbon: RIBEYE deletion abolishes ribbons in retinal synapses and disrupts neurotransmitter release. *EMBO J.* 35:1098–1114.
23. Thoreson, W. B., K. Rabl, …, R. Heidelberger. 2004. A highly Ca^{2+}-sensitive pool of vesicles contributes to linearity at the rod photoreceptor ribbon synapse. *Neuron.* 42:595–605.
24. von Gersdorff, H., E. Vardi, …, P. Sterling. 1996. Evidence that vesicles on the synaptic ribbon of retinal bipolar neurons can be rapidly released. *Neuron.* 16:1221–1227.
25. Mehta, B., J. B. Ke, …, J. H. Singer. 2014. Global Ca^{2+} signaling drives ribbon-independent synaptic transmission at rod bipolar cell synapses. *J. Neurosci.* 34:6233–6244.
26. Chen, M., D. Križaj, and W. B. Thoreson. 2014. Intracellular calcium stores drive slow non-ribbon vesicle release from rod photoreceptors. *Front. Cell. Neurosci.* 8:20.
27. Luo, F., T. Bacaj, and T. C. Südhof. 2015. Synaptotagmin-7 is essential for Ca^{2+}-triggered delayed asynchronous release but not for Ca^{2+}-dependent vesicle priming in retinal ribbon synapses. *J. Neurosci.* 35:11024–11033.
28. Heidelberger, R., and G. Matthews. 1992. Calcium influx and calcium current in single synaptic terminals of goldfish retinal bipolar neurons. *J. Physiol.* 447:235–256.
29. van Hook, M. J., and W. B. Thoreson. 2013. Simultaneous whole-cell recordings from photoreceptors and second-order neurons in an amphibian retinal slice preparation. *J. Vis. Exp.* http://dx.doi.org/10.3791/50007.
30. Heidelberger, R. 2001. ATP is required at an early step in compensatory endocytosis in synaptic terminals. *J. Neurosci.* 21:6467–6474.
31. Burrone, J., G. Neves, …, L. Lagnado. 2002. Endogenous calcium buffers regulate fast exocytosis in the synaptic terminal of retinal bipolar cells. *Neuron.* 33:101–112.
32. Singer, J. H., and J. S. Diamond. 2003. Sustained Ca^{2+} entry elicits transient postsynaptic currents at a retinal ribbon synapse. *J. Neurosci.* 23:10923–10933.
33. Matthews, G., and P. Sterling. 2008. Evidence that vesicles undergo compound fusion on the synaptic ribbon. *J. Neurosci.* 28:5403–5411.
34. Gomis, A., J. Burrone, and L. Lagnado. 1999. Two actions of calcium regulate the supply of releasable vesicles at the ribbon synapse of retinal bipolar cells. *J. Neurosci.* 19:6309–6317.
35. Zhou, Z. Y., Q. F. Wan, …, R. Heidelberger. 2006. Capacitance measurements in the mouse rod bipolar cell identify a pool of releasable synaptic vesicles. *J. Neurophysiol.* 96:2539–2548.
36. Lindau, M., and E. Neher. 1988. Patch-clamp techniques for time-resolved capacitance measurements in single cells. *Pflugers Arch.* 411:137–146.
37. Gillis, K. D. 1995. Techniques for membrane capacitance measurements. *In* Single-Channel Recordings. B. Sakmann and E. Neher, editors. Plenum Press, New York, NY, pp. 155–198.
38. Bartoletti, T. M., and W. B. Thoreson. 2011. Quantal amplitude at the cone ribbon synapse can be adjusted by changes in cytosolic glutamate. *Mol. Vis.* 17:920–931.
39. Curtis, L., P. Datta, …, R. Janz. 2010. Syntaxin 3B is essential for the exocytosis of synaptic vesicles in ribbon synapses of the retina. *Neuroscience.* 166:832–841.
40. Messler, P., H. Harz, and R. Uhl. 1996. Instrumentation for multiwavelengths excitation imaging. *J. Neurosci. Methods.* 69:137–147.
41. Wan, Q. F., E. Nixon, and R. Heidelberger. 2012. Regulation of presynaptic calcium in a mammalian synaptic terminal. *J. Neurophysiol.* 108:3059–3067.
42. van Hook, M. J., and W. B. Thoreson. 2014. Endogenous calcium buffering at photoreceptor synaptic terminals in salamander retina. *Synapse.* 68:518–528.
43. Wan, Q. F., Z. Y. Zhou, …, R. Heidelberger. 2010. SV2 acts via presynaptic calcium to regulate neurotransmitter release. *Neuron.* 66:884–895.
44. Horrigan, F. T., and R. J. Bookman. 1994. Releasable pools and the kinetics of exocytosis in adrenal chromaffin cells. *Neuron.* 13:1119–1129.
45. Wan, Q. F., A. Vila, …, R. Heidelberger. 2008. Synaptic vesicle dynamics in mouse rod bipolar cells. *Vis. Neurosci.* 25:523–533.
46. von Gersdorff, H., and G. Matthews. 1994. Inhibition of endocytosis by elevated internal calcium in a synaptic terminal. *Nature.* 370:652–655.
47. Rouze, N. C., and E. A. Schwartz. 1998. Continuous and transient vesicle cycling at a ribbon synapse. *J. Neurosci.* 18:8614–8624.
48. Hanson, P. I., R. Roth, …, J. E. Heuser. 1997. Structure and conformational changes in NSF and its membrane receptor complexes visualized by quick-freeze/deep-etch electron microscopy. *Cell.* 90:523–535.
49. von Rüden, L., and E. Neher. 1993. A Ca-dependent early step in the release of catecholamines from adrenal chromaffin cells. *Science.* 262:1061–1065.
50. Llobet, A., A. Cooke, and L. Lagnado. 2003. Exocytosis at the ribbon synapse of retinal bipolar cells studied in patches of presynaptic membrane. *J. Neurosci.* 23:2706–2714.
51. Zenisek, D., V. Davila, …, W. Almers. 2003. Imaging calcium entry sites and ribbon structures in two presynaptic cells. *J. Neurosci.* 23:2538–2548.
52. von Gersdorff, H., and G. Matthews. 1997. Depletion and replenishment of vesicle pools at a ribbon-type synaptic terminal. *J. Neurosci.* 17:1919–1927.
53. Graydon, C. W., J. Zhang, …, J. S. Diamond. 2014. Passive diffusion as a mechanism underlying ribbon synapse vesicle release and resupply. *J. Neurosci.* 34:8948–8962.
54. Beaumont, V., A. Llobet, and L. Lagnado. 2005. Expansion of calcium microdomains regulates fast exocytosis at a ribbon synapse. *Proc. Natl. Acad. Sci. USA.* 102:10700–10705.
55. Morgans, C. W., J. H. Brandstätter, …, H. Wässle. 1996. A SNARE complex containing syntaxin 3 is present in ribbon synapses of the retina. *J. Neurosci.* 16:6713–6721.
56. Curtis, L. B., B. Doneske, …, R. Janz. 2008. Syntaxin 3b is a t-SNARE specific for ribbon synapses of the retina. *J. Comp. Neurol.* 510:550–559.
57. Sutton, R. B., D. Fasshauer, …, A. T. Brunger. 1998. Crystal structure of a SNARE complex involved in synaptic exocytosis at 2.4 Å resolution. *Nature.* 395:347–353.
58. Walter, A. M., K. Wiederhold, …, J. B. Sørensen. 2010. Synaptobrevin N-terminally bound to syntaxin-SNAP-25 defines the primed vesicle state in regulated exocytosis. *J. Cell Biol.* 188:401–413.
59. Francis, A. A., B. Mehta, and D. Zenisek. 2011. Development of new peptide-based tools for studying synaptic ribbon function. *J. Neurophysiol.* 106:1028–1037.
60. DeBello, W. M., V. O'Connor, …, G. J. Augustine. 1995. SNAP-mediated protein-protein interactions essential for neurotransmitter release. *Nature.* 373:626–630.
61. Hayashi, T., H. McMahon, …, H. Niemann. 1994. Synaptic vesicle membrane fusion complex: action of clostridial neurotoxins on assembly. *EMBO J.* 13:5051–5061.

62. Sherry, D. M., R. Mitchell, …, B. du Plessis. 2006. Distribution of plasma membrane-associated syntaxins 1 through 4 indicates distinct trafficking functions in the synaptic layers of the mouse retina. *BMC Neurosci.* 7:54.

63. Cadetti, L., T. M. Bartoletti, and W. B. Thoreson. 2008. Quantal mEPSCs and residual glutamate: how horizontal cell responses are shaped at the photoreceptor ribbon synapse. *Eur. J. Neurosci.* 27:2575–2586.

64. Cadetti, L., D. Tranchina, and W. B. Thoreson. 2005. A comparison of release kinetics and glutamate receptor properties in shaping rod-cone differences in EPSC kinetics in the salamander retina. *J. Physiol.* 569:773–788.

65. Thoreson, W. B., M. J. van Hook, …, C. Curto. 2016. Modeling and measurement of vesicle pools at the cone ribbon synapse: changes in release probability are solely responsible for voltage-dependent changes in release. *Synapse.* 70:1–14.

66. van Hook, M. J., C. M. Parmelee, …, W. B. Thoreson. 2014. Calmodulin enhances ribbon replenishment and shapes filtering of synaptic transmission by cone photoreceptors. *J. Gen. Physiol.* 144: 357–378.

67. Oesch, N. W., and J. S. Diamond. 2011. Ribbon synapses compute temporal contrast and encode luminance in retinal rod bipolar cells. *Nat. Neurosci.* 14:1555–1561.

68. Heidelberger, R., C. Heinemann, …, G. Matthews. 1994. Calcium dependence of the rate of exocytosis in a synaptic terminal. *Nature.* 371:513–515.

69. von Gersdorff, H., and G. Matthews. 1996. Calcium-dependent inactivation of calcium current in synaptic terminals of retinal bipolar neurons. *J. Neurosci.* 16:115–122.

70. Bunt, A. H. 1971. Enzymatic digestion of synaptic ribbons in amphibian retinal photoreceptors. *Brain Res.* 25:571–577.

71. Parsons, T. D., and P. Sterling. 2003. Synaptic ribbon. Conveyor belt or safety belt? *Neuron.* 37:379–382.

72. Vaithianathan, T., and G. Matthews. 2014. Visualizing synaptic vesicle turnover and pool refilling driven by calcium nanodomains at presynaptic active zones of ribbon synapses. *Proc. Natl. Acad. Sci. USA.* 111:8655–8660.

73. Vaithianathan, T., D. Henry, …, G. Matthews. 2016. Nanoscale dynamics of synaptic vesicle trafficking and fusion at the presynaptic active zone. *eLife.* 5:e13245.

74. Jahn, R., and R. H. Scheller. 2006. SNAREs—engines for membrane fusion. *Nat. Rev. Mol. Cell Biol.* 7:631–643.

75. Südhof, T. C., and J. Rizo. 2011. Synaptic vesicle exocytosis. *Cold Spring Harb. Perspect. Biol.* 3:a005637.

76. Wadel, K., E. Neher, and T. Sakaba. 2007. The coupling between synaptic vesicles and Ca^{2+} channels determines fast neurotransmitter release. *Neuron.* 53:563–575.

77. Young, S. M., Jr., and E. Neher. 2009. Synaptotagmin has an essential function in synaptic vesicle positioning for synchronous release in addition to its role as a calcium sensor. *Neuron.* 63:482–496.

78. Chen, Z., B. Das, …, S. M. Young, Jr. 2015. Ca^{2+} channel to synaptic vesicle distance accounts for the readily releasable pool kinetics at a functionally mature auditory synapse. *J. Neurosci.* 35:2083–2100.

79. Zenisek, D., N. K. Horst, …, G. Matthews. 2004. Visualizing synaptic ribbons in the living cell. *J. Neurosci.* 24:9752–9759.

80. LoGiudice, L., P. Sterling, and G. Matthews. 2008. Mobility and turnover of vesicles at the synaptic ribbon. *J. Neurosci.* 28:3150–3158.

81. Matthews, G., and P. Fuchs. 2010. The diverse roles of ribbon synapses in sensory neurotransmission. *Nat. Rev. Neurosci.* 11:812–822.

82. Ma, C., L. Su, …, J. Rizo. 2013. Reconstitution of the vital functions of Munc18 and Munc13 in neurotransmitter release. *Science.* 339:421–425.

83. Rizo, J., and J. Xu. 2015. The synaptic vesicle release machinery. *Annu. Rev. Biophys.* 44:339–367.

84. Han, J., K. Pluhackova, and R. A. Böckmann. 2017. The multifaceted role of SNARE proteins in membrane fusion. *Front. Physiol.* 8:5.

85. Sudhof, T. C. 2004. The synaptic vesicle cycle. *Annu. Rev. Neurosci.* 27:509–547.

86. Südhof, T. C. 2012. The presynaptic active zone. *Neuron.* 75:11–25.

87. Cooper, B., M. Hemmerlein, …, F. Varoqueaux. 2012. Munc13-independent vesicle priming at mouse photoreceptor ribbon synapses. *J. Neurosci.* 32:8040–8052.

88. Liu, X., R. Heidelberger, and R. Janz. 2014. Phosphorylation of syntaxin 3B by CaMKII regulates the formation of t-SNARE complexes. *Mol. Cell. Neurosci.* 60:53–62.

89. Lv, C., W. J. Stewart, …, D. Zenisek. 2016. Synaptic ribbons require ribeye for electron density, proper synaptic localization, and recruitment of calcium channels. *Cell Reports.* 15:2784–2795.

90. Takamori, S., M. Holt, …, R. Jahn. 2006. Molecular anatomy of a trafficking organelle. *Cell.* 127:831–846.

91. Sinha, R., S. Ahmed, …, J. Klingauf. 2011. Two synaptobrevin molecules are sufficient for vesicle fusion in central nervous system synapses. *Proc. Natl. Acad. Sci. USA.* 108:14318–14323.

92. Hua, Y., and R. H. Scheller. 2001. Three SNARE complexes cooperate to mediate membrane fusion. *Proc. Natl. Acad. Sci. USA.* 98:8065–8070.

93. van den Bogaart, G., M. G. Holt, …, R. Jahn. 2010. One SNARE complex is sufficient for membrane fusion. *Nat. Struct. Mol. Biol.* 17:358–364.

94. Brochetta, C., R. Suzuki, …, U. Blank. 2014. Munc18-2 and syntaxin 3 control distinct essential steps in mast cell degranulation. *J. Immunol.* 192:41–51.

95. Blank, U., B. Cyprien, …, N. Varin-Blank. 2002. SNAREs and associated regulators in the control of exocytosis in the RBL-2H3 mast cell line. *Mol. Immunol.* 38:1341–1345.

96. Alvarez de Toledo, G., and J. M. Fernandez. 1990. Compound versus multigranular exocytosis in peritoneal mast cells. *J. Gen. Physiol.* 95:397–409.

97. Fields, R. D., and M. H. Ellisman. 1985. Synaptic morphology and differences in sensitivity. *Science.* 228:197–199.

98. Mehta, B., J. Snellman, …, D. Zenisek. 2013. Synaptic ribbons influence the size and frequency of miniature-like evoked postsynaptic currents. *Neuron.* 77:516–527.

99. Rudolph, S., M. C. Tsai, …, J. I. Wadiche. 2015. The ubiquitous nature of multivesicular release. *Trends Neurosci.* 38:428–438.